Delayed loss of stability of periodic travelling waves: Insights from the analysis of essential spectra

Journal of Theoretical Biology 595 (2024) 111945

Contents lists available at ScienceDirect

Journal of Theoretical Biology

journal homepage: www.elsevier.com/locate/yjtbi

Delayed loss of stability of periodic travelling waves: Insights from the analysis of essential spectra

Lukas Eigentler [a,b,c,*], Mattia Sensi [d]

[a] Evolutionary Biology Department, Universität Bielefeld, Konsequenz 45, 33615 Bielefeld, Germany
[b] Warwick Mathematics Institute, University of Warwick, Coventry CV4 7AL, United Kingdom
[c] Zeeman Institute for Systems Biology & Infectious Disease Epidemiology Research, University of Warwick, Coventry CV4 7AL, United Kingdom
[d] Department of Mathematical Sciences "G. L. Lagrange", Politecnico di Torino, Corso Duca degli Abruzzi 24, 10129 Torino, Italy

ARTICLE INFO

Keywords:
Periodic travelling waves
Wavetrains
Plane waves
Delayed loss of stability
Vegetation patterns

ABSTRACT

Periodic travelling waves (PTW) are a common solution type of partial differential equations. Such models exhibit multistability of PTWs, typically visualised through the Busse balloon, and parameter changes typically lead to a cascade of wavelength changes through the Busse balloon. In the past, the stability boundaries of the Busse balloon have been used to predict such wavelength changes. Here, motivated by anecdotal evidence from previous work, we provide compelling evidence that the Busse balloon provides insufficient information to predict wavelength changes due to a delayed loss of stability phenomenon. Using two different reaction–advection–diffusion systems, we relate the delay that occurs between the crossing of a stability boundary in the Busse balloon and the occurrence of a wavelength change to features of the essential spectrum of the destabilised PTW. This leads to a predictive framework that can estimate the order of magnitude of such a time delay, which provides a novel "early warning sign" for pattern destabilisation. We illustrate the implementation of the predictive framework to predict under what conditions a wavelength change of a PTW occurs.

1. Introduction

Partial Differential Equations (PDEs) are ubiquitous in the field of mathematical modelling of spatio-temporal natural phenomena. In particular, an ever-growing number of researchers devote their attention to pattern formation in various PDE models to understand self-organisation in a wide range of fields, ranging from ecology (Rietkerk and van de Koppel, 2008), to cell biology (Dzianach et al., 2019), to solar dynamics (Pontin and Priest, 2022), and more.

This work focuses on a specific type of spatio-temporal pattern in PDE systems: periodic travelling waves (PTWs), sometimes referred to as wavetrains or plane waves. PTWs describe spatio-temporal patterns which are periodic in space and migrate at a constant velocity through the domain (Kopell and Howard, 1973). Such solutions have been observed in a wide range of PDE models, including but not limited to dynamics of dryland vegetation patterns (Sherratt, 2005), intertidal mussel beds (Bennett and Sherratt, 2018a), hydrothermal waves (van Hecke, 2003), solar cycles (Proctor et al., 2000), and pulses in excitable systems (Bordyugov et al., 2010). We note that PTW also occur in integrodifferential equations (Gourley et al., 2001; Eigentler and Sherratt, 2023), integrodifference equations (Kot, 1992; Britton, 1990), and individual based models (Sherratt, 1996; Degond et al., 2022). In this paper, our sole focus lies on PDE models on a one-dimensional space domain.

A remarkable feature of PDE models admitting PTWs is that they typically exhibit multistability of PTWs (Busse, 1978; Bastiaansen et al., 2018; Sherratt et al., 2021). This means that, assuming a sufficiently large or infinite spatial domain, if one PTW is stable for a given set of PDE parameters, then other PTWs with different emergent properties (e.g., wavelength, wavespeed, wavenumber) are also stable. PTW stability in one-dimensional space domains is a well-explored topic: the stability of a PTW can be determined through a calculation of its essential spectrum. Results are typically visualised through the Busse balloon (Busse, 1978) which indicates regions of PTW stability in a two-dimensional parameter plane, spanned by the main PDE bifurcation parameter and one of the emergent properties of the PTWs (see Fig. 3.1A for an example).

Spatio-temporal patterns described by PTWs often occur in systems that undergo exogeneous change (e.g. climate change impact on dryland vegetation patterns) (United Nations Convention to Combat Desertification, 2017). It is thus crucial to completely understand how PTWs, and their stability, evolve under changing PDE parameters. Under changing parameters, PTWs preserve their wavelength as long

* Corresponding author at: Warwick Mathematics Institute, University of Warwick, Coventry CV4 7AL, United Kingdom.
E-mail address: lukas.eigentler@warwick.ac.uk (L. Eigentler).

https://doi.org/10.1016/j.jtbi.2024.111945
Received 21 November 2023; Received in revised form 26 June 2024; Accepted 7 September 2024
Available online 16 September 2024

as the PTW of that wavelength remains stable. Wavelength changes can only occur after a PTW crosses a stability boundary in the Busse balloon. This has important consequences, because wavelength changes typically cannot be reversed by simply reversing the parameter change. This is a well known feature, known as hysteresis (Sherratt, 2013a). The exact dynamics of how crossing a stability boundary leads to destabilisation remain underexplored. Nevertheless, it is known that the type of stability boundary, which is classified by the shape of the essential spectrum at the boundary (see e.g., Sherratt (2013b), van der Stelt et al. (2013) for a detailed overview) a PTW crosses upon destabilisation affects the dynamics: Eckhaus boundaries lead to a wavelength change, while Hopf boundaries can lead to oscillations of pattern peaks with the wavelength being preserved in the vicinity of the stability boundary (Dagbovie and Sherratt, 2014; Bennett and Sherratt, 2018b).

However, even for Eckhaus stability boundaries, numerical results highlight that destabilisation is not instant upon crossing the stability boundary, and that PTWs can persist for biologically significant times after losing stability, exhibiting a *delayed loss of stability*, before they eventually undergo a wavelength change (Sherratt, 2013a, 2016). This highlights that stability boundaries in the Busse balloon do not provide sufficient information to predict wavelength changes of PTWs. Current evidence of this delayed loss of stability that induces a time delay between the crossing of a stability boundary in the Busse balloon and the occurrence of a wavelength change is anecdotal and descriptive, rather than predictive, and based on piecewise constant bifurcation parameter regimes only (Sherratt, 2013a, 2016). It is worth noting, however, that there exists theory on delayed loss of stability phenomena in ODE systems (De Maesschalck, 2008; De Maesschalck and Schecter, 2016; Liu, 2000; Neishtadt, 1987; Kaklamanos et al., 2023) and theory which links the rate of change of a parameter to transient behaviour after crossing a bifurcation in non-PTW-admitting PDE systems (Dalwadi and Pearce, 2023).

In this paper, we focus on a novel predictive approach to quantify this delayed loss of stability. We develop a predictive understanding of the order of magnitude of the time delay that occurs between a PTW destabilisation at an Eckhaus stability boundary and the occurrence of an irreversible wavelength change. We show that the precise dynamics of parameter changes have a strong influence on when a wavelength change occurs and link these dynamics to the essential spectra of the PTWs. We develop this theory using a model describing dryland vegetation stripes. Further, we show that all results also apply to a model for intertidal mussel beds and thus argue that the predictive framework applies to all PTWs of PDE models that lose their stability at an Eckhaus stability boundary.

The paper is structured as follows. We describe the models used to obtain our results in Section 2. In Section 3, we review the state-of-the-art knowledge on how essential spectra and the Busse balloon are used to predict wavelength changes of PTW, but also highlight why this information is not always sufficient. We use Section 4 to provide information on how the delayed loss of stability between PTW destabilisation and wavelength changes depends on the system's parameter values, but highlight that parameter values alone cannot predict wavelength changes. Section 5 contains the main result of this paper: the theory and practical implementation of a predictive method, based on the PTWs' essential spectra, that provides information on the order of magnitude of the delayed loss of stability between PTW destabilisation and wavelength changes. We discuss the importance of our results in Section 6.

2. The model

We consider the reaction–advection–diffusion system

$$\frac{\partial \boldsymbol{u}}{\partial t} = \boldsymbol{f}(\boldsymbol{u};\boldsymbol{\alpha}) + \boldsymbol{N}\frac{\partial \boldsymbol{u}}{\partial x} + \boldsymbol{D}\frac{\partial^2 \boldsymbol{u}}{\partial x^2}, \quad x \in \mathbb{R}, t \geq 0. \tag{1}$$

Model densities are represented by $\boldsymbol{u} = (u_1, \dots, u_n) \in \mathbb{R}^n$. Non-spatial dynamics are accounted for by the function $\boldsymbol{f}(\boldsymbol{u};\boldsymbol{\alpha}) = (f_1(\boldsymbol{u};\boldsymbol{\alpha}), \dots, f_n(\boldsymbol{u};\boldsymbol{\alpha}))$, where $\boldsymbol{\alpha} = (A, A_1, A_2, \dots) \in \mathbb{R}_+^m$ is a set of model parameters, and A denotes the main bifurcation parameter of the system. Spatial dynamics comprise diffusion of model densities with diffusion coefficients $\boldsymbol{D} = \mathrm{diag}(d_1, \dots d_n) \in \mathbb{R}_+^n$, and advection of model densities with speeds $\boldsymbol{N} = \mathrm{diag}(v_1, \dots, v_n)$. We assume the following on the function $\boldsymbol{f}$ and the parameters $\boldsymbol{N}$ and $\boldsymbol{D}$:

- Let $\overline{\boldsymbol{u}}(\boldsymbol{\alpha})$ be a positive, spatially uniform equilibrium of (1), i.e., $f(\overline{\boldsymbol{u}};\boldsymbol{\alpha}) = 0$.
- Let $\overline{\boldsymbol{u}}(\boldsymbol{\alpha})$ be stable for $A > A_H \in \mathbb{R}$ and lose its stability at a Turing–Hopf bifurcation at $A = A_H$.
- Let (1) admit stable PTW solutions for $A \in A_{\mathrm{PTW}} = [A_L, A_U]$, where $A_U \geq A_H$.
  A Periodic travelling wave (PTW) solution of (1) is a solution $\boldsymbol{U}(z) = \boldsymbol{u}(x,t), z = x - ct, c \in \mathbb{R}$ which satisfies
  $$0 = \boldsymbol{f}(\boldsymbol{U};\boldsymbol{\alpha}) + (c\boldsymbol{I}_n + \boldsymbol{N})\frac{\mathrm{d}\boldsymbol{U}}{\mathrm{d}z} + \boldsymbol{D}\frac{\mathrm{d}^2\boldsymbol{U}}{\mathrm{d}z^2}, \tag{2}$$
  where $\boldsymbol{I_n}$ is the $n \times n$ identity matrix. This travelling wave system is obtained from (1) through transformation into travelling wave coordinates, $z = x - ct$.
- Let stability boundaries in the system's Busse balloon be of Eckhaus type.

In essence, the last two bullet points ensure the occurrence of PTWs that lose their stability at an Eckhaus boundary; this is the setting for which we aim to explore the concept of a delayed loss of stability in more detail. The first two bullet points provide us with a way to construct PTWs through numerical continuation (see Sherratt (2012, 2013b), Eigentler and Sherratt (2020) for a detailed explanation).

Below, we present a mathematical model of pattern formation in dryland plant ecosystems that fits into model class (1) and satisfies the aforementioned hypotheses. This system will be used to visualise our results throughout the main text. Moreover, in Appendix C.1, we present a second model of class (1) for which we repeat our analysis to provide evidence that results presented in this paper apply to all models fitting into class (1).

2.1. The extended Klausmeier model for dryland vegetation patterns

Throughout the main text of the paper, we use the *extended Klausmeier model* to develop and illustrate our results. The model was first proposed by Klausmeier (1999) to describe vegetation stripes that form parallel to contours on gentle slopes in dryland ecosystems. For a detailed overview of the underlying ecological dynamics and other modelling approaches, we refer to the comprehensive reviews by Gandhi et al. (2019), Meron (2016). The nondimenionalised (see Klausmeier (1999), Sherratt (2005) for the nondimensionalisation[1]) model we consider in this paper is

$$\frac{\partial u}{\partial t} = \overbrace{u^2 w}^{\text{plant growth}} - \overbrace{Bu}^{\text{plant loss}} + \overbrace{\frac{\partial^2 u}{\partial x^2}}^{\text{plant dispersal}}, \tag{3a}$$

$$\frac{\partial w}{\partial t} = \underbrace{A}_{\text{rainfall}} - \underbrace{w}_{\text{evaporation}} - \underbrace{u^2 w}_{\substack{\text{water uptake}\\ \text{by plants}}} + \underbrace{v\frac{\partial w}{\partial x}}_{\substack{\text{water flow}\\ \text{downhill}}} + \underbrace{D\frac{\partial^2 w}{\partial x^2}}_{\text{water diffusion}}. \tag{3b}$$

The densities $u(x,t)$ and $w(x,t)$ describe the plant density and water density, respectively, at space point $x \in \mathbb{R}$ and time $t \geq 0$. Water diffusion was not part of the system originally, but is a widely used addition

[1] The nondimensionalisations in these papers do not include $D = d_1/d_2$, which describes the ratio between the water diffusion coefficient $d_2 > 0$, and the plant diffusion coefficient $d_1 > 0$.

(e.g. (Siteur et al., 2014; Zelnik et al., 2013; Eigentler, 2020)) which leads the model to be referred to as the *extended* Klausmeier model. Typically, the main bifurcation parameter of the model is the rainfall constant $A \geq 0$, since it represents the environmental stress acting on the system. This model fits into the general framework (1) by setting (with a slight abuse of notation) $\boldsymbol{u} = (u, w), \boldsymbol{\alpha} = (A, B), \boldsymbol{N} = (0, \nu), \boldsymbol{D} = (1, D)$, and $\boldsymbol{f}(\boldsymbol{u}; \boldsymbol{\alpha}) = (u^2 w - Bu, A - w - u^2 w)$. The analysis of PTW solutions of the extended Klausmeier model representing vegetation stripes has a rich history (e.g., (Bastiaansen et al. (2018), Bennett and Sherratt (2018b), Consolo et al. (2019), Consolo and Valenti (2019), Marasco et al. (2014), Sherratt (2010, 2005, 2011, 2013a,c,d,e), Sherratt and Lord (2007), Siero (2018), Siero et al. (2019), Siteur et al. (2014), Wang and Zhang (2019, 2018))) and thus the model is an ideal example to investigate the delayed loss of stability property. Unless otherwise stated we use $B = 0.45, \nu = 182.5, D = 500$ (Klausmeier, 1999; Siteur et al., 2014).

3. The Busse balloon provides insufficient predictions of wavelength changes

It is a well known feature of models of class (1) that multistability of PTW solutions occurs (Busse, 1978; Bastiaansen et al., 2018; Sherratt et al., 2021). That is, if for a set of PDE parameters $\alpha = \alpha^*$, (1) admits a stable PTW solution with the wavelength–wavespeed–wavenumber triple $(L, c, k) = (L^*, c^*, k^*)$, then, for the same PDE parameters $\alpha = \alpha^*$, other PTW solutions (forming a continuum if the domain is infinite) with different emergent properties ($L \neq L^*$, $c \neq c^*$, $k \neq k^*$) are also stable.[2] This information can be neatly summarised visually through a stability diagram, often termed the *Busse balloon* (Busse, 1978), see e.g. Fig. 3.1A, in a parameter plane spanned by the main bifurcation parameter of the PDE system (A), and one of the PTW's emergent properties (here c). Note that wavespeed, wavelength and wavenumber of a PTW are related. As a consequence, Busse balloons can also be visualised with any of the other quantities on the y-axis.

To construct a Busse balloon, information on PTW stability is required. For a given PTW, i.e. the solution of the PTW system (2) for a fixed PDE parameter set $\boldsymbol{\alpha}$ and wavespeed c, its stability is determined by its essential spectrum (Fig. 3.1B). Practically (for full details see Rademacher et al. (2007), Sherratt (2012, 2013b)), the essential spectrum $\Lambda \subset \mathbb{C}$ of a PTW describes the growth rate (to linear order) of perturbations to the PTW. Thus, if $\mu := \max_{\lambda \in \Lambda, \lambda \neq 0}(\Re(\lambda)) < 0$, the corresponding PTW is stable, and unstable otherwise. The origin $\lambda = 0 \in \Lambda$ is excluded from this stability definition, as it is always part of the essential spectrum due to the translation invariance of PTWs.

Fig. 3.1A shows the Busse balloon for the Klausmeier model for a specific choice of the model parameters (see the caption for the precise values). In particular, it visualises the Eckhaus stability boundary (red) which splits the PTW existence region (bounded by blue curves) into stable and unstable PTWs. Thus, for any given wavelength, the intersection of the wavelength contour (black) with the stability boundary determines the value of the bifurcation parameter $A = A_{\text{stab}}$ at which the PTW loses its stability. Here, the stability boundary is of Eckhaus type (meaning, the essential spectrum evolves towards instability through a change in curvature at the origin; see Sherratt (2013b), Bennett and Sherratt (2018b), Dagbovie and Sherratt (2014) for more information on types of stability boundaries). Intuitively, one would expect the PTW to undergo a wavelength change immediately upon crossing the boundary (Dagbovie and Sherratt, 2014). However, in previous papers, a delayed loss of stability phenomenon has been highlighted. More precisely, it has been shown that, provided that the bifurcation parameter is varied at a sufficiently large rate in a stepwise manner, wavelength changes only occur well beyond the stability boundary, and with a time delay (Sherratt, 2013a, 2016).

[2] The exception is the location of a Turing–Hopf bifurcation, at which, if supercritical, there is only one stable PTW.

There is a possibility that these observations are the results of numerical errors that occur close to the stability boundary. However, we were able to independently verify this phenomenon using our numerical methods (Fig. 3.2). For this, we initialised simulations with a stable pattern (constructed using numerical continuation) located close to the stability boundary at $A = A_0$, where $0 < A_0 - A_{\text{stab}} \ll 1$. Here, we chose a wavelength $L = 20$ PTW at $A = 1.7$ with the stability boundary being at $A_{\text{stab}} \approx 1.69$. After an initial calibration phase of 100 time units, we instantaneously changed the bifurcation parameter to $A = A_{\text{target}} < A_{\text{stab}}$, continued the simulation and recorded the time delay t_{delay} between crossing a stability boundary and the occurrence of a wavelength change. Significantly, this independent verification also revealed that the length of the delay can differ by several order of magnitudes depending on the value of A_{target} (Fig. 3.2). The remainder of the paper aims to characterise why such an order of magnitude difference in the time delay t_{delay} exists and how the order of magnitude of such a delay can be predicted.

Before proceeding to characterise the delayed loss of stability phenomenon in more detail, we remark that the delay is *approximately memoryless* (relative to the order of magnitude difference reported for parameter changes) with respect to the dynamics that occur before crossing the stability boundary in the Busse balloon (Appendix A and Fig. A.1). Combined, this provides compelling – yet purely *descriptive* – numerical evidence of a delayed loss of stability phenomenon, with the observed delays spanning several orders of magnitude depending on parameter values. This means that, under some parameter regimes, PTWs which are unstable according to the Busse balloon can be realised as transients over ecologically relevant timescales (Fig. 3.2). Therefore, the Busse balloon does not provide sufficient information on when wavelength changes occur in these cases. Below, we investigate this phenomenon further and develop more *predictive* information on what determines the order of magnitude of wavelength change delays.

4. Wavelength changes and their dependence on parameter distance to stability boundaries

Having established that wavelength changes do not occur instantaneously after crossing an Eckhaus stability boundary, we first quantified how the order of magnitude of the time delay t_{delay} depends on the distance of the bifurcation parameter to the stability boundary. To do so, we repeated our numerical simulations described in the previous section for a wide range of A_{target}. To allow comparison to other parameter change regimes (see below), we denote the bifurcation parameter at which the wavelength change occurs by A_{change}. Here, $A_{\text{change}} = A_{\text{target}}$ due to the choice of the change regime of the bifurcation parameter. Our simulations revealed that changes of the bifurcation parameter to values further from the stability boundary (i.e. lower values of A_{target}) decrease the time delay between the parameter change and the wavelength change (Fig. 4.1A, red). Moreover, we recorded that the time delay t_{delay} approximately scales with the distance to the stability boundary $A_{\text{stab}} - A_{\text{target}}$ through $t_{\text{delay}} \sim (A_{\text{stab}} - A_{\text{target}})^{-2} = (A_{\text{stab}} - A_{\text{change}})^{-2}$. We thus conclude that the order of magnitude of the time delay t_{delay} is determined by the distance of the bifurcation parameter to the stability boundary.

The aforementioned numerical investigation, albeit useful for our understanding of the mechanisms underlying the delayed loss of stability, is rather unnatural from a biological point of view. In real-world ecosystems, changes of environmental conditions are rarely instantaneous. Rather, changes are often gradual. We therefore repeated our simulations with a regime in which the bifurcation parameter decreased linearly from its initial value $A_0 = 1.7$ after the initial calibration phase, i.e. $A(t) = A_0$ for $t \leq 100$ and $A(t) = A_0 - mt$, for some $m > 0$, for $t > 100$. Note that, in contrast to the previous simulations, the value of the bifurcation parameter at which the wavelength change occurs (A_{change}) is an emergent property of the simulation rather than an input. Our simulations with this parameter regime revealed a strikingly

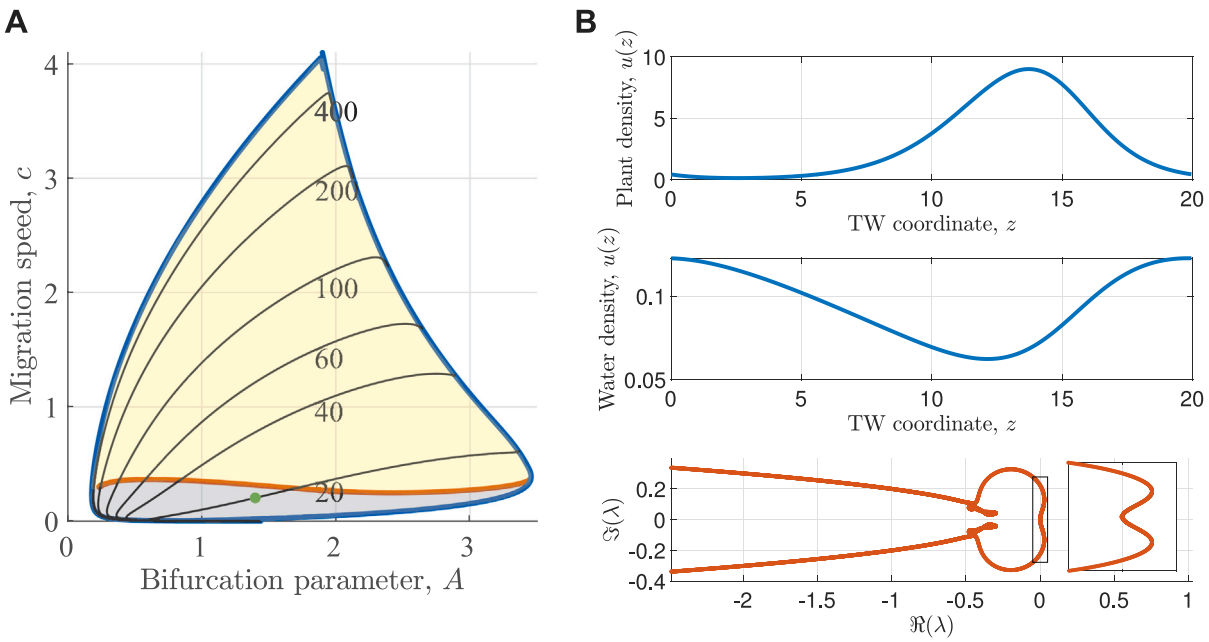

Fig. 3.1. Busse balloon and essential spectra. A: Busse balloon of the Klausmeier model (3). Shaded regions visualise regions of pattern existence, split into stable (yellow) and unstable (grey) patterns. Existence boundaries are shown in blue, stability boundaries in red. Annotated solid black curves show wavelength contours. The green dot on the $L = 20$ contour indicates the location of the solution shown in **B**. **B:** One period of an example PTW for $A = 1.4$ and $L = 20$ (top and centre). Its essential spectrum is shown in the bottom panel, with the inset zooming into the region around the imaginary axis indicated by the black box; notice that the essential spectrum trespasses in the region $\Re(\lambda) > 0$. Other parameter values are $B = 0.45, \nu = 182.5, D = 500$ across both figures.

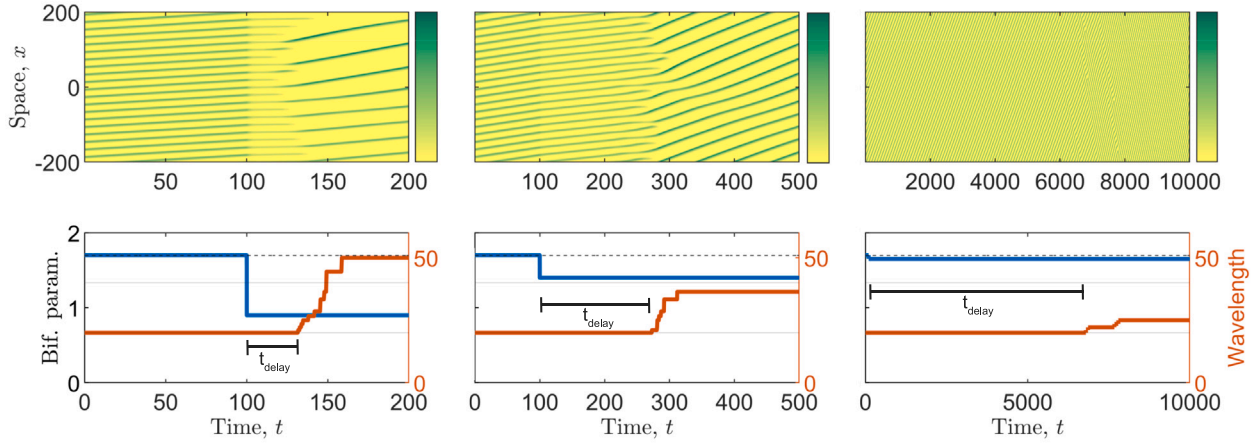

Fig. 3.2. Delay examples. The top panel in each of the rows shows the contour plot of the plant density u of system (3) in the time–space parameter plane. The simulation is initialised with a stable PTW constructed using numerical continuation. The bifurcation parameter (blue curve in bottom panel) is kept at its initial value for 100 time units before it is abruptly decreased to $A = A_{target}$ beyond the stability boundary. Here, $A_{target} = 0.9$ (left), $A_{target} = 1.4$ (middle), and $A_{target} = 1.65$ (right). A wavelength change (red curve in bottom panel) only occurs after a time delay t_{delay}. Note the different limits on the time axes. In all three cases, $A_0 = 1.7$ and $A_{stab} \approx 1.69$. Other parameter values are $B = 0.45, \nu = 182.5, D = 500$ across all figures.

similar relation between the time delay t_{delay} and the distance to the stability boundary at the wavelength change $(A_{stab} - A_{change})$ compared with the regime of instantaneous changes in the bifurcation parameter. Again, we observed that $t_{delay} \sim (A_{stab} - A_{change})^{-2}$ (Fig. 4.1B, blue). However, for fixed distance to the stability boundary, the time delays in the instantaneous change regime were much shorter (up to one order of magnitude) than in the constant rate of change regime (Fig. 4.1).

The comparison of the two regimes above highlights that there is a clear qualitative relation between how far a PTW can cross a stability boundary and the order of magnitude of the time delay before a wavelength change occurs. However, the quantitative differences between the two parameter change regimes highlight that the distance to the stability boundary alone has little predictive power. Instead, we hypothesised that the distance to the stability boundary during the entirety of the delay phase must be accounted for. To test this hypothesis, we defined the *accumulated distance from the stability boundary* as

$$\overline{A}(t) := \int_{t_{stab}}^{t} A(\tau)\,\mathrm{d}\tau, \quad t \geq t_{stab} \tag{4}$$

where t_{stab} denotes the time at which the bifurcation parameter last crossed the stability boundary to push the PTW into an unstable regime. If our hypothesis regarding the predictive power of the accumulated distance from the stability boundary $\overline{A}(t)$ was true, then we would see no dependence of the time delay t_{delay} on $\overline{A}(t_{stab} + t_{delay})$. We compared the accumulated distance from the stability boundary at the time of the wavelength change, $\overline{A}(t_{stab} + t_{delay})$ with the time delay t_{delay} for both previously described parameter change regimes. Most significantly, we discovered that there is a clear relation between the accumulated distance from the stability boundary and the time delay

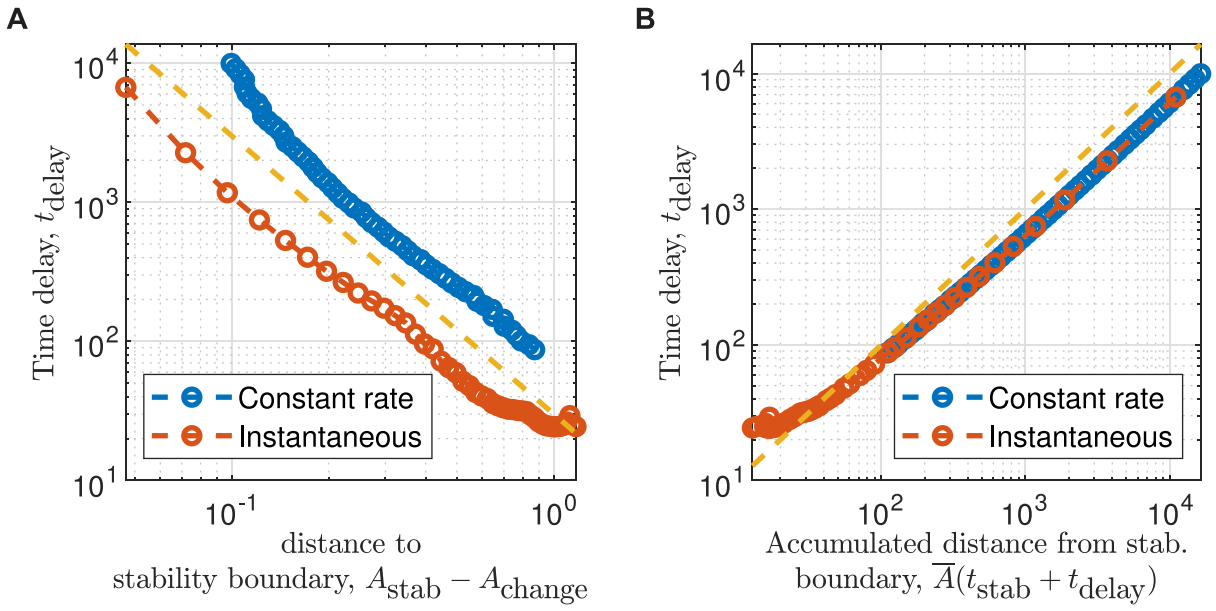

Fig. 4.1. Time delay in relation to bifurcation parameter changes. A: The relation between the time delay t_{delay} and the distance of the bifurcation parameter A from the stability boundary at the time of the wavelength change is shown for an instantaneous parameter change to a target value A_{target} (red), and for a regime in which A decreases at constant rate m (blue) with each datapoint corresponding to a different value of m. The dashed lines have slope −2. **B**: The relation between the time delay t_{delay} and the accumulated distance from the stability boundary at the time of the wavelength change, $\overline{A}(t_{\text{stab}} + t_{\text{delay}})$, is shown for both parameter change regimes. The dashed line has slope 1. Other parameter values are $B = 0.45, \nu = 182.5, D = 500$.

and thus rejected our hypothesis on the predictive power of accumulated distance from the stability boundary. However, we also found excellent quantitative agreement across the data from both parameter change regimes (Fig. 4.1C). Moreover, we detected that the relation between the time delay and the accumulated distance from the stability boundary is approximately $t_{\text{delay}} \sim \overline{A}(t_{\text{stab}} + t_{\text{delay}})$. These numerical data show that the order of magnitude of the time delay t_{delay} is determined by the accumulated distance from the stability boundary $\overline{A}(t_{\text{stab}} + t_{\text{delay}})$, independent of the parameter change regime. Yet, the implicit nature of the relationship does not provide any predictive information on the order of magnitude of the time delay of any wavelength change.

5. The maximum real part of the essential spectrum determines the order of magnitude of the delay

The previous section revealed a clear relation between the time delay t_{delay} before a wavelength change occurs after a PTW crosses a stability boundary and the bifurcation parameter's accumulated distance from the stability boundary. However, this relation possesses no predictive power because both these quantities depend on the time delay. Nevertheless, the relation highlights the importance of considering the details of solution dynamics during the entirety of the delay phase, rather than solely focussing on the wavelength change itself.

Given that the model's parameter values alone hold no predictive power on wavelength changes, we next turned our attention to the essential spectra of the destabilised PTWs. As described above, the essential spectrum of a PTW determines the behaviour (up to linear order) of perturbations to the PTW, and therefore provides information on the linear stability of the PTW. An example spectrum is shown in Fig. 3.1B and a stack of spectra for different values of A that were obtained for PTWs with wavelength $L = 20$ and is shown in Fig. 5.1A. The maximum real part of the essential spectrum, $\mu(A) := \max_{\lambda \in \Lambda, \lambda \neq 0}(\Re(\lambda(A)))$ (red curve in Fig. 5.1A) is of particular significance because it describes the linear growth rate of the fastest growing perturbation of the form $\overline{U} \sim \exp(\lambda t)$ to the underlying PTW. We therefore hypothesised that given the previously reported relation between time delay t_{delay} and bifurcation parameter A, the delay and the spectra should be related through $t_{\text{delay}} \sim \mu(A_{\text{change}})^{-1}$. This is in part motivated by general theory (e.g. Hastings et al. (2018)) and dryland vegetation pattern-specific results (Eigentler and Sherratt, 2019) on transients which highlight that unstable states whose leading eigenvalues feature a small but positive real part can lead to the preservation of intrinsically unstable states over ecologically relevant timescales.

To test this hypothesis, we returned to the numerical data for the two different parameter change regimes investigated in the previous section and calculated the essential spectra for the PTWs at the parameter values at which they underwent a wavelength change. To do so, we implemented the numerical continuation method developed by Rademacher et al. (2007) (but see also Sherratt (2012, 2013b)) in AUTO-07p (Doedel et al., 2012). For both parameter change regimes, we found that indeed $t_{\text{delay}} \sim \mu(A_{\text{change}})^{-1}$ (Fig. 5.2A). Thus, the order of magnitude of the time delay t_{delay} is affected by how far the spectrum of the unstable PTW extends beyond the imaginary axis in the complex plane.

Despite the clear relation between the time delay t_{delay} and the maximum real part of the essential spectrum of the unstable PTW at the wavelength change, $\mu(A_{\text{change}})$ in both parameter change regimes, there were significant (up to one order of magnitude) differences across the two regimes. This highlighted that the spectrum at the wavelength change alone does not possess sufficient power to predict the order of magnitude of the time delay. Motivated by the results of the previous section, we instead considered the maximum real parts of the essential spectra of the PTWs during the entirety of the delay phase. Similar to the previous section, we defined the *accumulated maximal instability* as

$$\overline{\mu}(A(t)) = \int_{t_{\text{stab}}}^{t} \mu(\tau) d\tau, \quad t \geq t_{\text{stab}}. \tag{5}$$

As in definition (4), we highlight that t_{stab} denotes the *last* time the system crossed a stability boundary from a stable to an unstable regime. We compared the accumulated maximal instability at a wavelength change, i.e. $\overline{\mu}_{\text{change}} := \overline{\mu}(A_{\text{change}})$, with the time delay t_{delay} for both parameter change regimes. In both cases, we found that there exists no clear relation between the accumulated maximal instability and the time delay (Fig. 5.2C). Moreover, we observed that wavelength changes occur within a small interval $I_{\overline{\mu}_{\text{change}}}$, i.e. when $\overline{\mu}_{\text{change}} \in I_{\overline{\mu}_{\text{change}}}$. In our

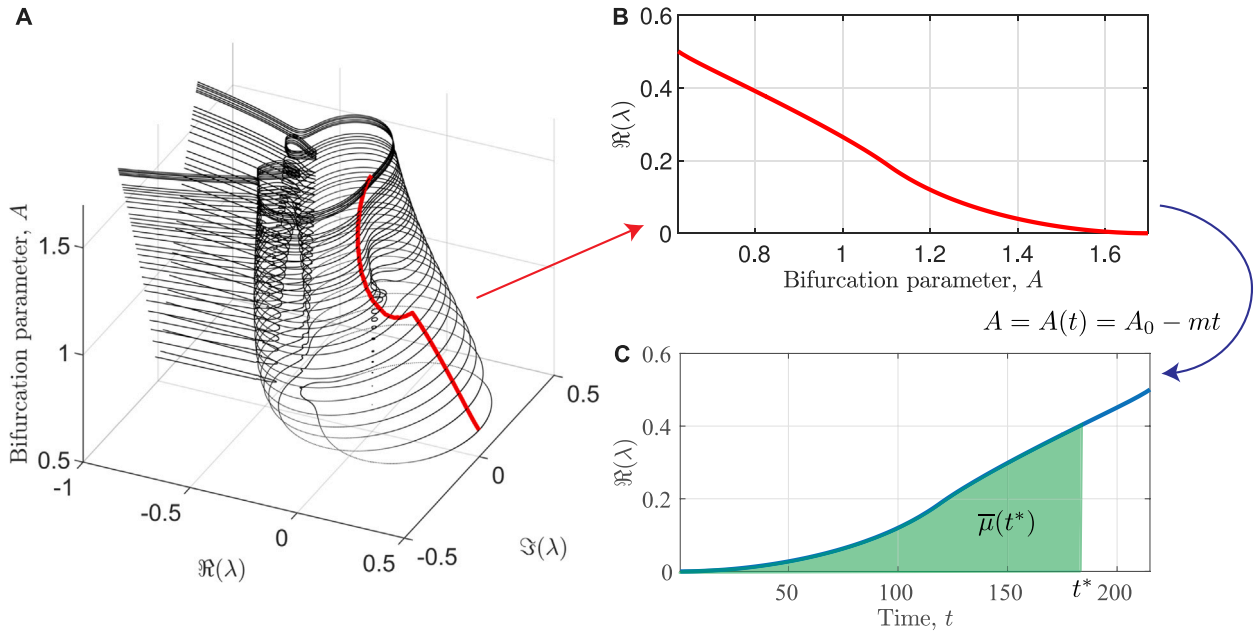

Fig. 5.1. Accumulated maximal instability. **A**: Spectra of PTW with wavelength $L = 20$ of system (3) are shown as a stack with the bifurcation parameter A on the z-axis. The red curve traces the maximum real parts of the spectra. Note that if the maximum occurs away from the real axis, the maximum is not unique due to the occurrence of complex conjugates. Only the maximum occurring in the $\Im(\lambda) < 0$ plane is shown. **B**: The maximum real part of the spectra (red curve in **A**) is plotted against the bifurcation parameter A. **C**: The maximum real part of the spectra is plotted against time. The curve is obtained by transforming the x-axis in **B** using the relation $A = A(t)$. Here, $A(t) = A_0 - mt$ with $A_0 = 1.7$, $m = 0.005$. The green shaded area indicates how the accumulated maximum instability $\overline{\mu}(t^*)$ is calculated for a specific value $t = t^*$. Other parameter values are $B = 0.45, \nu = 182.5, D = 500$.

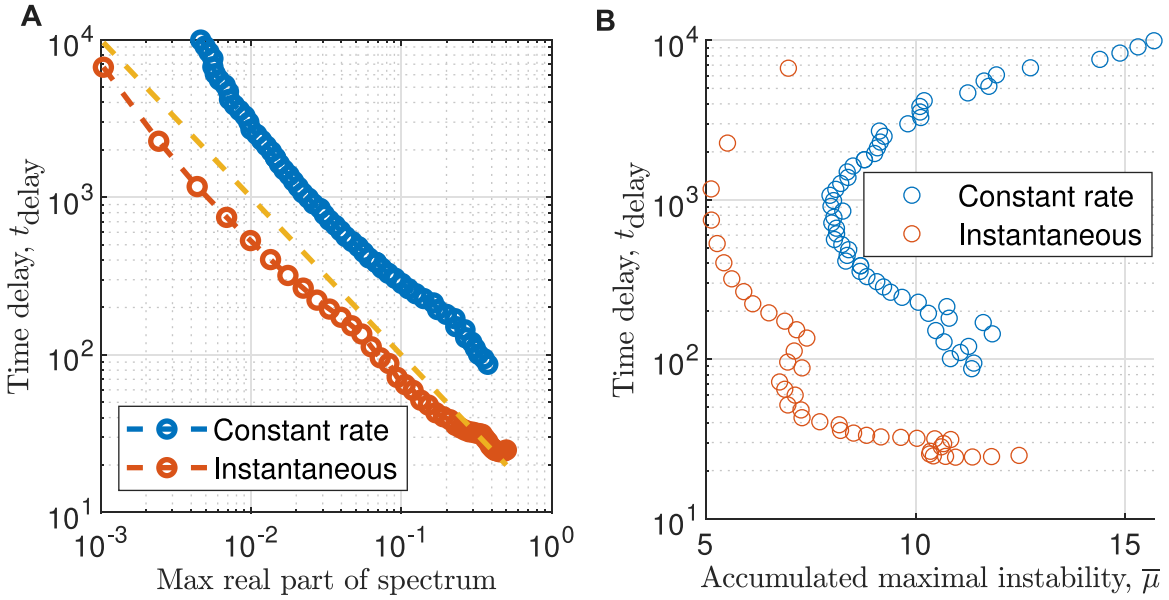

Fig. 5.2. Time delay of wavelength change in relation to the maximum real part of the essential spectrum. **A**: The time delay of a wavelength change that occurs after crossing a stability boundary is compared with the maximum real part of the essential spectrum of the unstable solution at which the wavelength change occurs for instantaneous changes of the bifurcation parameter (red), and constant rates of change of the bifurcation parameter (blue). The dashed line has slope −1. **B**: The time delay is compared with the accumulated maximal instability for both parameter change regimes. Other parameter values are $B = 0.45, \nu = 182.5, D = 500$.

data, we observed wavelength changes within $I_{\overline{\mu}_{\text{change}}} \approx [5, 16]$. While this does not provide us with one critical value of $\overline{\mu}_{\text{change}}$ at which the wavelength change occurs, the interval's range (in terms of order of magnitude) is much smaller than the range of the maximum real parts of spectra recorded at the wavelength changes (these spectra range from 10^{-3} to $5 \cdot 10^{-1}$ in our data). We thus conclude that we can obtain an order of magnitude prediction of how long after crossing a stability boundary a PTW undergoes a wavelength change by tracking the order of magnitude of the accumulated maximal instability $\overline{\mu}$ until $\overline{\mu} \in I_{\overline{\mu}_{\text{change}}}$. We detail the procedure in the next section.

5.1. Delay predictions in practice

The previous section revealed that wavelength changes of PTWs after crossing a stability boundary occur when the accumulated maximal instability $\overline{\mu}(t)$ reaches the interval $I_{\overline{\mu}_{\text{change}}}$. The predictive power of this result can be exploited as follows. Consider a stable PTW of

interest and a bifurcation parameter change regime $A(t)$ that pushes the PTW across a stability boundary at $t = t_{\text{stab}} > 0$. Then, $\overline{\mu}(A(t))$ can be calculated by computing the essential spectra of the PTW along the wavelength contour it follows under the parameter change regime $A(t)$. The quantity $\overline{\mu}(t)$ can be examined over time and a prediction of the time delay t_{delay} can be made by determining the order of magnitude of the time t at which $\overline{\mu}(t) \in I_{\overline{\mu}}$. Recall that for our data, we observed $I_{\overline{\mu}_{\text{change}}} \approx [5, 16]$. For our predictive framework, we therefore chose $\overline{\mu}(t) = 10$ as the critical threshold. Using any other value within $I_{\overline{\mu}_{\text{change}}}$ would not have changed the order of magnitude of the predicted delay t_{delay}.

Fig. 5.3 shows two examples of the predictor with comparisons to numerical simulations. Fig. 5.3A shows a prediction for a wavelength $L = 20$ PTW in a regime in which the bifurcation parameter decays at a constant rate from an initial value close to the stability boundary, i.e. $A(t) = A_0 - mt$ with $m = 0.005$. The prediction is compared with a numerical simulation, initialised at $A = A_0 = 1.7$ with a PTW constructed through numerical continuation. Fig. 5.3B shows a prediction for the same PTW, but under a slower change regime $A(t) = A_0 - mt$ with $m = 0.0001$. In both cases, there is excellent agreement between the order of magnitude of the delay prediction and the order of magnitude of the observed delay in a numerical simulation. We note that we tested the predictive method for other parameter change regimes and found similarly excellent agreement in all cases (Fig. B.1).

The predictive framework is not only capable of predicting the time delay between a solution trajectory crossing a stability boundary in the Busse balloon and the occurrence of a wavelength change, but can also indicate to what extent solution changes in response to changes of the bifurcation parameter are reversible. Systems of type (1) that admit PTWs are known to feature hysteresis (Sherratt, 2013a). That is, wavelength changes that occur due to a decrease of the bifurcation parameter, cannot be reversed by simply reversing the changes to the bifurcation parameters. In the past, the stability boundaries in the Busse balloon have often been used to define critical thresholds that cause such irreversible changes (Sherratt, 2013b; Bastiaansen et al., 2020; van der Stelt et al., 2013). However, the analysis in the preceding sections highlights that wavelength changes do not necessarily occur at the Busse balloon's stability boundary because a delay phase may occur. Our predictive framework is therefore able to characterise parameter change regimes that only cause reversible solution changes by characterising the accumulated maximal instability of these parameter changes.

For the characterisation of the reversibility of parameter change regimes, it is essential to recall that in the definition of the accumulated maximal instability $\overline{\mu}$ in (5), the quantity t_{stab} refers to the *last* time the bifurcation parameter crossed a stability boundary from a stable into a unstable regime. That is, the accumulated maximal instability is memoryless to previous delay phases and must be reset whenever parameters return into a stable regime. We highlight this property through the following counterexample, visualised in Fig. 5.4, in which not resetting $\overline{\mu}$ leads to an inaccurate prediction of a wavelength change. For this, we initiated a model simulation with a wavelength $L = 20$ PTW at $A = A_0 = 1.75$. We then varied the bifurcation parameter A through the following periodic regime. First, we decreased A at rate $m = 10^{-4}$ for $t^* = 1800$ time units, i.e. $A(t) = A_0 - mt$ for $2(n-1)t^* < t \leq (2n-1)t^*, n \in \mathbb{N}$. We then increased A at the same rate for the next t^* time units, i.e. $A(t) = A(t^*) + mt$ for $(2n-1)t^* < t \leq 2nt^*, n \in \mathbb{N}$. This periodic regime caused the system to spend time in both the stable and unstable regime for the $L = 20$ PTW during each oscillation. We recorded (i) the accumulated maximal instability $\overline{\mu}$ as defined by (5) where t_{stab} denotes the *last* time the parameters transitioned into an unstable regime and $\overline{\mu}$ is reset to $\overline{\mu} = 0$ whenever a transition to a stable regime occurs; and (ii) the accumulated maximal instability without reset, whose definition was identical to that of $\overline{\mu}$, with the exception that t_{stab} denotes the *first* time the parameter regime enters an unstable region. If we assumed that the accumulated maximal instability $\overline{\mu}$ never resets, then our predictive framework would predict a wavelength change to occur within the first few oscillations due to an assumed additive effect of the maximal instability across the oscillations (Fig. 5.4 bottom left; red). However, as shown in the simulation of this parameter change regime in Fig. 5.4 (top right), and predicted by $\overline{\mu}$ with resets (Fig. 5.4 bottom left; blue), no wavelength change occurs. This highlights that the process is memoryless: the PTW "forgets" its excursion in the unstable regime as soon as it re-enters the stable part of the Busse balloon. We note that we have chosen a parameter regime in which the excursions into stable regions last for a sufficiently long time and are sufficiently far away from the stability boundary. We have not attempted to define the meaning of the term "sufficiently" in this context, but argue that an exploration of this is an important aspect of future work.

6. Discussion

Parameter changes in PDE systems admitting PTWs often cause a cascade of transitions between PTWs of different wavelengths (Rietkerk et al., 2021). Wavelength changes are typically associated with PTW destabilisation when a PTW crosses a stability boundary in the Busse balloon (Bastiaansen et al., 2018). However, previous work has noted a delayed loss of stability phenomenon (Sherratt, 2016, 2013a). That is, there is a time delay between the crossing of a stability boundary and the occurrence of a wavelength change. Such delays have only been recorded for piecewise constant parameter change regime and all reports have been purely descriptive; they were noted as an aside when focussing on other research questions (Sherratt, 2013a, 2016). In this paper, we have developed a predictive tool to determine the order of magnitude of the time delay between the crossing of a stability boundary and the occurrence of a wavelength change. Moreover, we present strong evidence that our predictive scheme applies to any parameter change regime and any PTW that loses its stability at an Eckhaus stability boundary.

A predictive understanding of wavelength changes affecting PTWs is of crucial importance. This is because PDE systems admitting PTWs exhibit hysteresis and wavelength changes of PTWs cannot be reversed by simply reversing the parameter change that has occurred (Sherratt, 2013a; van der Stelt et al., 2013; Siero et al., 2019; von Hardenberg et al., 2001; Meron et al., 2004). Rather, a much larger change of the bifurcation parameter would be required to revert the system to its original wavelength. Thus wavelength transitions are examples of a tipping point in the sense that the PDE solution undergoes an almost instantaneous wavelength change after a long period of wavelength conservation (Fig. 3.2).

We note that there exists some confusion about the notion of tipping points in relation to PTWs. Pattern formation is sometimes attributed to be a mechanism to avoid tipping in the sense that it prevents the disappearance of a model density (Rietkerk et al., 2021; Pinto-Ramos et al., 2023). Here, following Bastiaansen et al. (2018), Bennett and Sherratt (2018b), we describe wavelength changes as a type of tipping. In the past, predictions of such tipping points for PTWs have solely relied on the location of stability boundaries in the Busse balloon (Sherratt, 2013b; Bastiaansen et al., 2020; van der Stelt et al., 2013). However, the observation of a delayed loss of stability phenomenon which can last for significant timescales (Section 3) highlights that the Busse balloon provides insufficient information for predicting the occurrence of a wavelength change. Rather, we highlight that a sufficient "amount" of instability, quantified by the notion of the accumulated maximal instability that is based on maximum real part of the essential spectrum of a unstable PTW, needs to accumulate before a wavelength change occurs (Section 5). Significantly, we show that this notion of the critical "amount" of the instability is identical across different parameter change regimes (Fig. 5.2B) and even across different PDE systems (Appendix C and Fig. C.3). From an ecological point of view, our results thus also add to the list of "early warning signals" that are

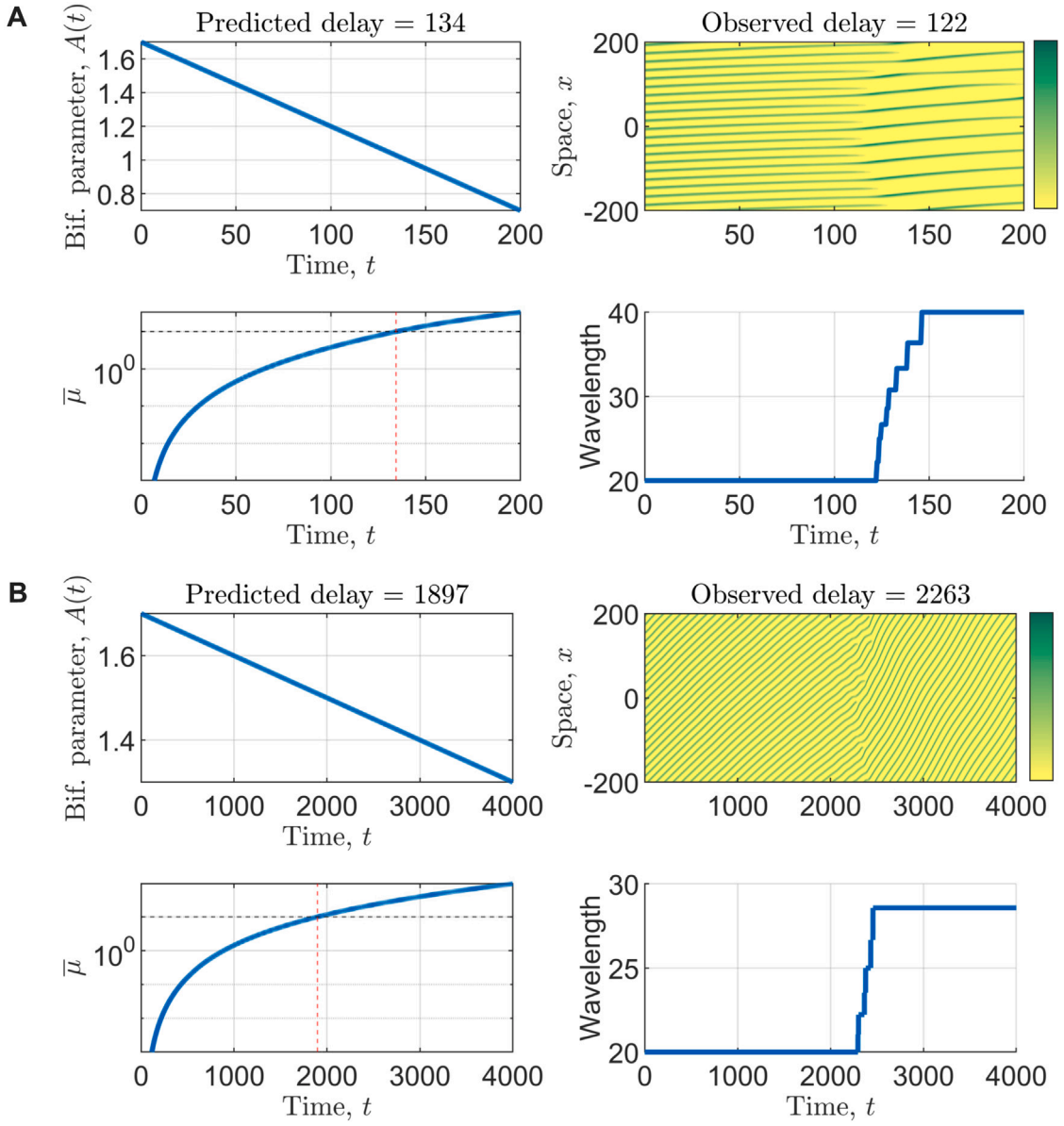

Fig. 5.3. Examples of delay predictions. A, B: Two predictions of the time delay with comparisons to the observed delay are shown. In both parts, the top left panel shows the changing bifurcation parameter over time. The bottom left panel shows the accumulated maximal instability. The black dashed line shows the critical prediction threshold $\overline{\mu} = 10$. The dashed red line shows the predicted time delay based on the $\overline{\mu}$ curve crossing the prediction threshold $\overline{\mu} = 10$. The top right panel shows the simulation outcome in the time–space plane. The bottom right panel shows the observed wavelength in the simulation over time. The rates of change of the bifurcation parameter are $m = 0.005$ in **A**, and $m = 0.0001$ in **B**. Other parameter values are $B = 0.45, \nu = 182.5, D = 500$.

used to detect tipping points, including wavelength transitions, before they occur (Scheffer et al., 2009; Kéfi et al., 2014; Dakos et al., 2011).

Despite our claim of the wide applicability of our results, it is important to emphasise that we developed our theory only for PTWs that lose their stability at an Eckhaus stability boundary. Models admitting PTWs can also feature Hopf stability boundaries (e.g., (Dagbovie and Sherratt, 2014; Bennett and Sherratt, 2018b; Eigentler and Sherratt, 2020)); the type of stability boundary is determined by *how* the essential spectrum crosses the imaginary axis (see Sherratt (2013b), van der Stelt et al. (2013) for more information). Previous studies have focussed on examining the different impacts of those two types of stability boundaries on PTW dynamics. While destabilisations of PTWs due to Eckhaus stability boundaries lead to wavelength changes (after a time delay), PTWs that are destabilised at a Hopf stability boundary preserve their wavelength and instead feature alternating oscillations in the pattern peaks provided parameters stay close to the stability boundary (Dagbovie and Sherratt, 2014; Bennett and Sherratt, 2018b). While Hopf-destabilised PTWs can also undergo a wavelength change (Eigentler and Sherratt, 2020), we are not aware of any comprehensive understanding of what causes wavelength changes in these cases. We view such an understanding as an essential precursor before being able to characterise the (potential) occurrence of a delayed loss of stability phenomenon and have therefore focussed solely on PTW that lose their stability at Eckhaus boundaries.

Our analysis focussed on PDE models admitting PTW due to their wide applicability in ecology (Bennett and Sherratt, 2018b; Sherratt, 2005), fluid dynamics (van Hecke, 2003), magnetohydrodynamics (Proctor et al., 2000), and excitable systems (Bordyugov et al., 2010), among others. Nevertheless, delays in the loss of stability are not exclusive to PTWs, and it is therefore tempting to draw a parallelism to certain classes of ordinary differential equations (ODEs) (De Maesschalck, 2008; De Maesschalck and Schecter, 2016; Liu, 2000; Neishtadt, 1987). Recently, the role of the maximum eigenvalue in this context has been proven for a minimal system (Kaklamanos et al., 2023). Whereas

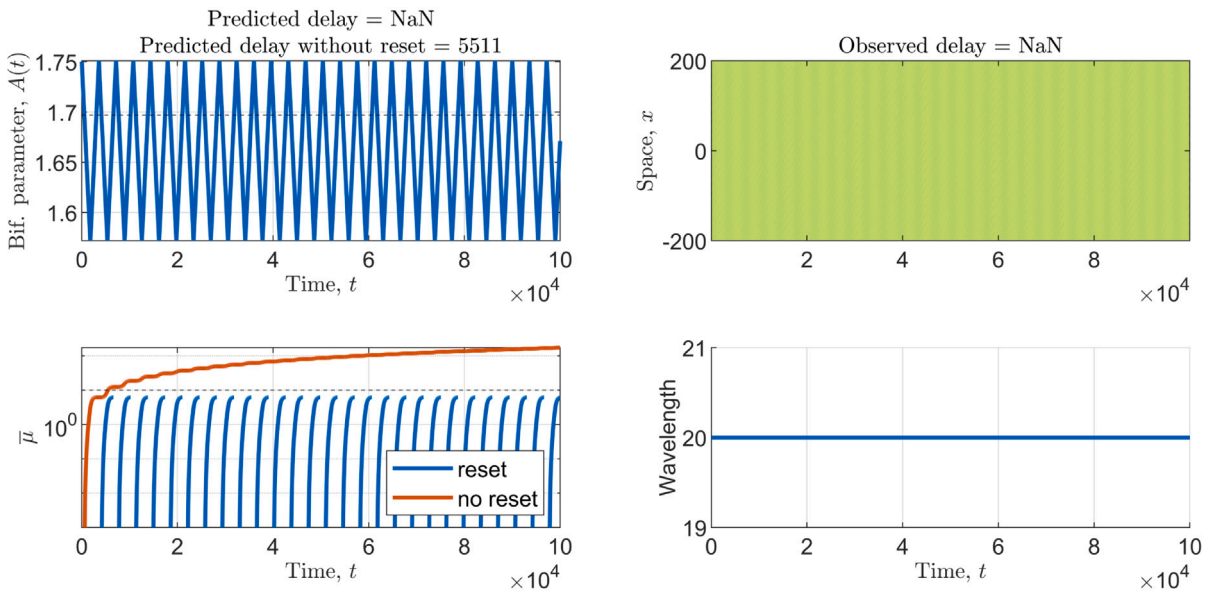

Fig. 5.4. Delay predictions reset in stable regions. This simulation highlights that it is essential to reset the value of the accumulated maximal instability $\bar{\mu}$ whenever parameter changes push the system back into a stable region (blue in bottom left panel). If $\bar{\mu}$ is not reset (red in bottom left panel), then this leads to inaccurate predictions of the occurrence of wavelength changes. For a full description of the figure panels, see Fig. 5.3; for a full description of the parameter change regime, see the main text. Other parameter values are $B = 0.45, \nu = 182.5, D = 500$.

previous theorems concerning the delayed loss of stability of singularly perturbed systems of ODEs assumed a complete separation of the eigenvalues (i.e., the eigenvalue which changes sign, and thus causes the loss of stability, should not intersect the other eigenvalues of the Jacobian), in Kaklamanos et al. (2023), the authors prove that in cases in which eigenvalues do intersect, the maximum eigenvalue throughout the dynamics characterises and determines the delay. This first result motivates further research in this direction. However, a major difference to the work presented in this paper is that systems of ODEs do not exhibit loss of memory like the PTW analysed in this paper: indeed, orbits which remain stable for longer periods are destabilised later, as the "accumulated stability" takes longer to be balanced by the "accumulated instability" De Maesschalck (2008), De Maesschalck and Schecter (2016). Moreover, also for PDEs, the phenomenon of delayed loss of stability has been reported for stationary patterns in a two-dimensional model for dryland vegetation patterns, and characterised using Fourier analysis for a select number of wavelength changes (Asch et al., 2024). Combined, we argue that future work should reconcile these approaches with the aim of developing a general understanding of the delayed loss of stability across a wide range of types of continuum models.

Moreover, we highlight that PTWs also occur in integrodifferential equations (Gourley et al., 2001; Eigentler and Sherratt, 2023), integrodifference equations (Kot, 1992; Britton, 1990), and individual based models (Sherratt, 1996; Degond et al., 2022). Theory for studying PTWs is best developed in PDE settings and, therefore, much less attention is currently being paid to other model types. In particular, we are not aware of tools to investigate PTW stability in any other model type. A characterisation of a delayed loss of stability phenomenon in these model types is a pressing, albeit challenging topic for future work.

The fact that all our observation and results in this paper are strongly tied to the essential spectrum, which is a first order approximation of the stability of a given PTW (Rademacher et al., 2007), provides a further important question for future work. Considering that we are observing the evolution of solutions in highly non-negligible intervals of time, higher order components might very well play a pivotal role. This leads to a considerably challenging question: would the essential spectrum calculated to higher order approximations provide sufficient additional information on the delayed loss of stability of PTWs to justify the expected cumbersome increase in computations and complexity? A nonlinear approach could also increase the accuracy of our predictive method. Here, we presented a method that provides an order of magnitude prediction of the delay between PTW destabilisation and occurrence of a wavelength change. However, more quantitative estimates would provide deeper insights into wavelength changes of PTWs.

Finally, we remark that this paper focusses only on the dynamics between pattern destabilisation and occurrence of a wavelength change. Crucially, it does not provide any information on the dynamics of the wavelength change itself. Characterising which new wavelength is chosen upon a PTW wavelength change is another underexplored question. Previous studies only highlighted significant differences between different model systems, ranging from small, almost gradual wavelength changes to period doubling regimes (Sherratt, 2016). Moreover, the various numerical simulations presented in this paper highlight that even within the same model, large differences between newly selected wavelengths occur depending on the parameter change regime. Moreover, our small number of simulations indicate that the time delay and the size of the wavelength change are inversely correlated (Figs. 5.3 and C.1). We thus hypothesise that, among other properties, the time delay that occurs due to a delayed loss of stability phenomenon plays are crucial role and we therefore view the results presented in this paper as an important precursor for this analysis.

CRediT authorship contribution statement

Lukas Eigentler: Writing – review & editing, Writing – original draft, Visualization, Software, Project administration, Methodology, Investigation, Formal analysis, Conceptualization. **Mattia Sensi:** Writing – review & editing, Writing – original draft, Project administration, Investigation, Formal analysis, Conceptualization.

Declaration of competing interest

The authors declare no conflicts of interest.

Data availability

Computational code used to obtain the results presented in this paper has been deposited in a Github repository which has been archived through Zenodo (Eigentler and Sensi, 2024).

Acknowledgements

L.E. was partly supported by the German Research Foundation (DFG) as part of the CRC TRR 212 (NC^3) – Project number 316099922.

M.S. was supported by the Italian Ministry for University and Research (MUR) through the PRIN 2020 project "Integrated Mathematical Approaches to Socio-Epidemiological Dynamics" (No. 2020JLWP23).

Appendix A. Approximate memorylessness of the delay

We obtained data on the approximate memorylessness of the delay t_{delay} with respect to the system dynamics before hitting a stability boundary as follows. We initiated each model simulation of system (3) with a PTW of wavelength $L = 20$ at $A = 2$. The initial condition was obtained through numerical continuation. We then decreased the bifurcation parameter A at a linear rate $-m$ before instantaneously switching it to $A = A_{\text{target}}$ upon hitting the stability boundary. We changed the linear decay rate $-m$ across different simulations and compared the observed time delay t_{delay}. In other words, we set $A = 2 - mt$ for $t < t_{\text{stab}}$, and $A = A_{\text{target}}$ for $t > t_{\text{stab}}$, where t_{stab} denotes the time at which $A = 2 - mt_{\text{stab}} = A_{\text{stab}}$. The results, visualised in Fig. A.1, highlight that the order of magnitude of the delay t_{delay} is unaffected by changes to the model dynamics that occur before crossing a stability boundary in the Busse balloon. We thus term this phenomenon *approximate memorylessness*.

Appendix B. More examples of delay predictions

In this section, we provide evidence that our method for predicting the time delay between PTW destabilisation and the occurrence of a wavelength change provides accurate order of magnitude estimates not only for the linear parameter change regimes described in the main text, but also for other parameter change regimes. In particular, we tested system (3) in the following cases:

- a decaying sinusoidal regime: $A(t) = 1.7 - mt(2 + \sin(t/50))$, $m = 0.0005$ (Fig. B.1A),
- a "change of direction" regime: $A(t) = 1.7 - mt$ for $t < t^*$, $A(t) = 1.7 - mt^* + m(t - t^*)$ for $t > t^*$, $m = 0.005$ (Fig. B.1B),
- a "zig zag" regime: $A(t) = 1.7 - mt$ for $t < t^* = 60$, $A(t) = 1.7 - mt^* + m(t - t^*)$ for $t^* < t < t^{**} = 115$, $A(t) = 1.7 - m(t^{**} - t^*) - m(t - (t^* + t^{**}))$ for $t^* < t < t^{**} = 115$, $m = 0.005$ (Fig. B.1C).

In all cases, we observed excellent agreement between the order of magnitude in the prediction and the numerical simulation.

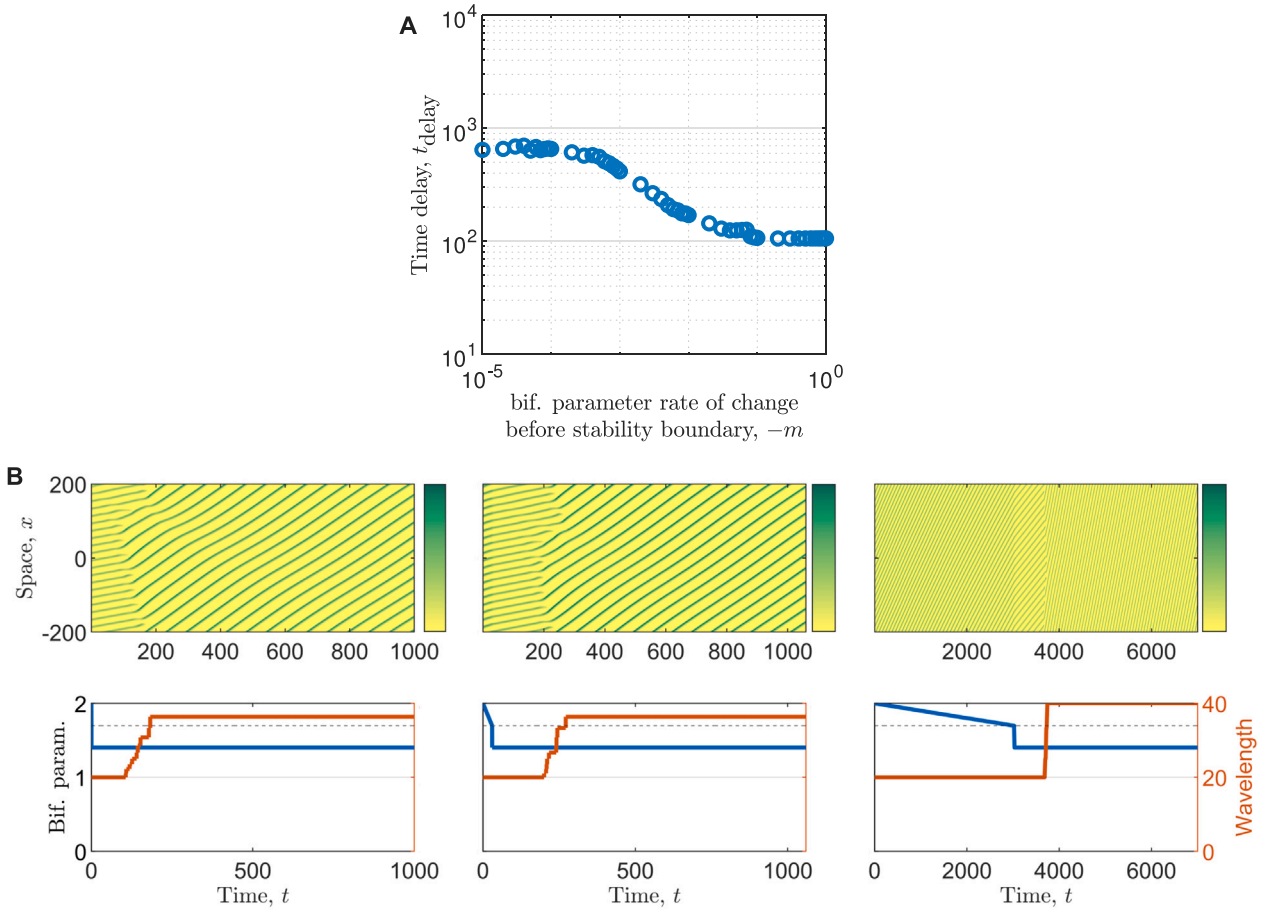

Fig. A.1. Approximate memorylessness of the delay. A: The time delays, t_{delay}, for simulations with varying rate of change ($-m$) of the bifurcation parameter before hitting the stability boundary ($A = 2 - mt$ for $t < t_{\text{stab}}$), and subsequent instantaneous switch to $A = A_{\text{target}} = 1.4$. Note that the delay is approximately independent of m (compared to the order of magnitude differences reported in Fig. 3.2). **B**: The three panels show the simulation results for three examples of the data shown in **A** for $m = 10^{-4}$ (left), $m = 10^{-2}$ (middle), $m = 1$ (right). Note the different limits on the time axes. Other parameter values are $B = 0.45, \nu = 182.5, D = 500$.

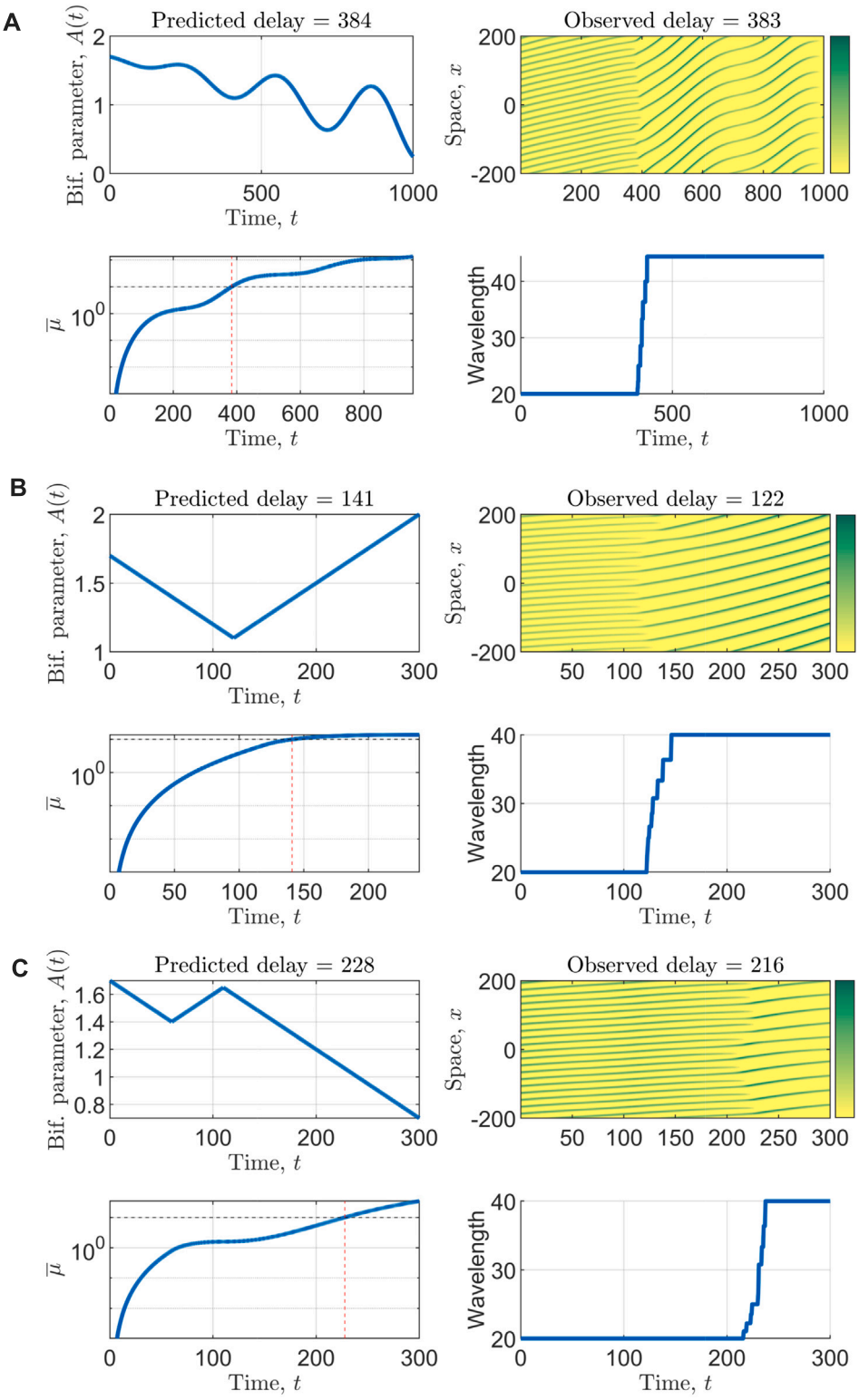

Fig. B.1. More examples of delay predictions in the Klausmeier model. For a full figure caption, see Fig. 5.3. For a description of the parameter change regimes used, see the supplemental text.

Appendix C. Results for the mussel model

C.1. The sediment accumulation model for intertidal mussel beds

We further to highlight that our results on the delayed loss of stability of PTWs applies to a range of different models admitting PTWs. We thus also consider the *sediment accumulation model* for intertidal mussel beds by Liu et al. (2012, 2014). For full details on the model, we refer to Sherratt (2016), Liu et al. (2012, 2014). More information on the ecological phenomenon, as well as an alternative mathematical model, can be found in van de Koppel et al. (2005), Shen and Wei (2020), Bennett and Sherratt (2018a), Sherratt and Mackenzie (2016).

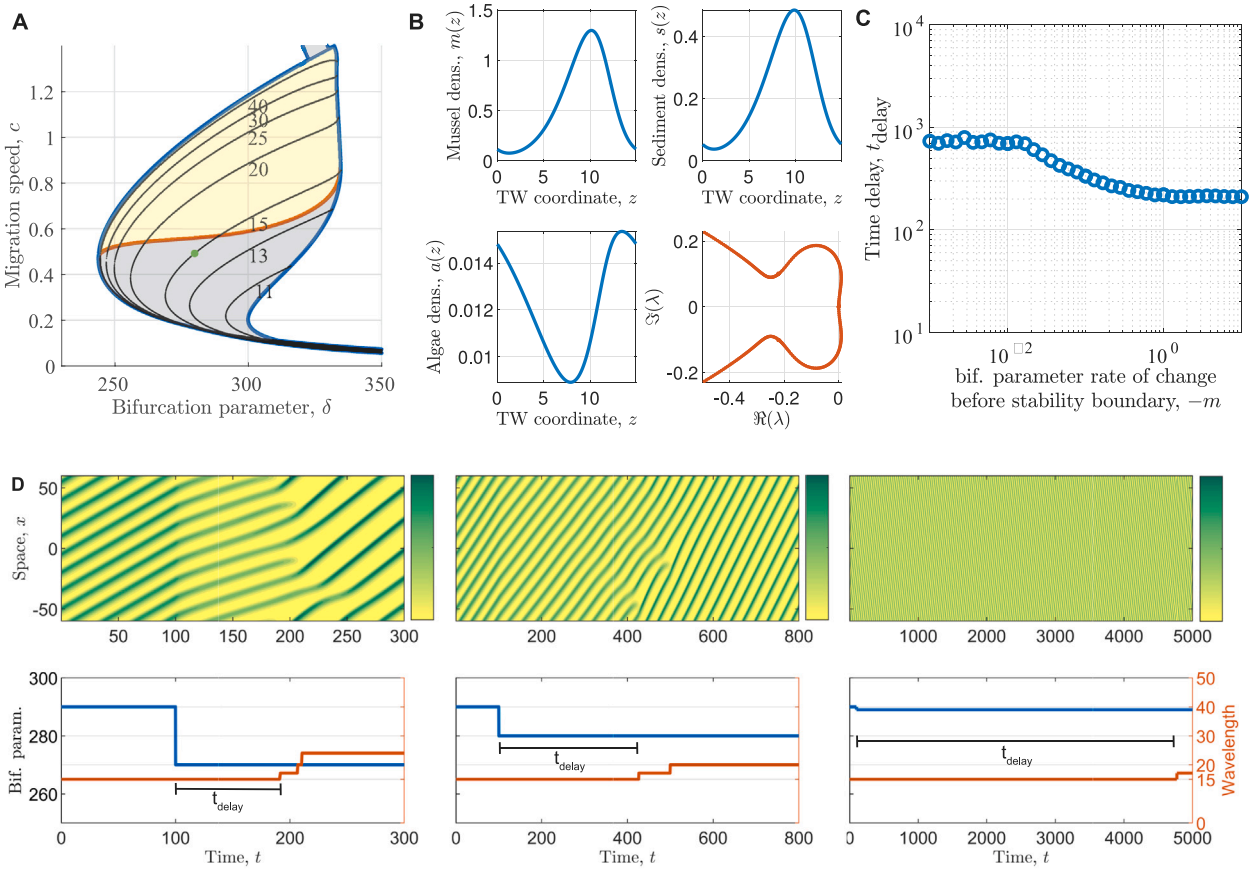

Fig. C.1. Busse balloon, essential spectra, and wavelength changes in the mussel model. A: Busse balloon of the sediment accumulation model for intertidal mussel beds system (6). Shaded regions visualise regions of pattern existence, split into stable (yellow) and unstable (grey) patterns. Existence boundaries are shown in blue, stability boundaries in red. Annotated solid black curves show wavelength contours. The green dot on the $L = 15$ contour indicates the location of the solution shown in **B**. Note that the blue curve in the top right region splitting stable into unstable regions is not a stability boundary. Rather, it is the location of a homoclinic orbit in which the stable solution terminates and leaves only one unstable solution remaining below the homoclinic orbit one stable and one unstable solution exist; for full details on the Busse balloon for this model see Sherratt (2016) **B:** One period only of an example PTW for $\delta = 280$ and $L = 15$ is shown (blue). Its essential spectrum (red) is shown in the bottom right panel. **C:** The time delays, t_{delay}, for simulations with varying rate of change ($-m$) of the bifurcation parameter before hitting the stability boundary ($\delta = 310 - mt$ for $t < t_{\text{stab}}$), and subsequent instantaneous switch to $\delta = \delta_{\text{target}} = 280$. Note that the delay is approximately independent of m (compared to the order of magnitude differences reported in **D**). **D:** Examples of wavelength changes occurring after a time delay. The top panel in each of the rows shows the contour plot of the mussel density in the time–space parameter plane. The simulation is initialised with a stable PTW constructed using numerical continuation. The bifurcation parameter (blue curve in bottom panel) is kept at its initial value $\delta_0 = 290$ for 100 time units before it is abruptly decreased to $\delta = \delta_{\text{target}}$ beyond the stability boundary, which is located at $\delta_{\text{stab}} \approx 299$. Here, $\delta_{\text{target}} = 270$ (left), $\delta_{\text{target}} = 280$ (middle), and $\delta_{\text{target}} = 289$ (right). A wavelength change (red curve in bottom panel) only occurs after a time delay t_{delay}. Note the different limits on the time axes. Other parameter values are $\epsilon = 50$, $\beta = 200$, $\eta = 0.1$, $\theta = 2.5$, $\nu = 360$, and $D = 1$ across all figures.

Suitably nondimensionalised (Liu et al. (2012)), the model we consider is

$$\frac{\partial m}{\partial t} = \overbrace{\frac{\delta a m(s+\eta)}{s+1}}^{\text{mussel growth}} - \overbrace{m}^{\text{mussel death}} + \overbrace{\frac{\partial^2 m}{\partial x^2}}^{\text{mussel dispersal}}, \tag{6a}$$

$$\frac{\partial s}{\partial t} = \underbrace{m}_{\text{sediment build-up}} - \underbrace{\theta s}_{\text{sediment erosion}} + \underbrace{D\frac{\partial^2 s}{\partial x^2}}_{\text{sediment dispersal}}, \tag{6b}$$

$$\frac{\partial a}{\partial t} = \underbrace{1+\varepsilon a}_{\substack{\text{transport from}\\ \text{upper water layers}}} - \underbrace{\frac{\beta a m(s+\eta)}{s+1}}_{\text{algae consumption}} + \underbrace{\nu\frac{\partial a}{\partial x}}_{\substack{\text{algae flow}\\ \text{with tide}}}. \tag{6c}$$

The densities $m(x,t), s(x,t)$, and $a(x,t)$ describe the mussel density, sediment density, and algae density, respectively at space point $x \in \mathbb{R}$ and time $t \geq 0$. The main bifurcation parameter of the system is the mussel growth rate $\delta \geq 0$. The system fits into our general framework (1) by setting $\boldsymbol{u} = (m,s,a), \boldsymbol{\alpha} = (\delta,\eta,\theta,\varepsilon,\beta), \boldsymbol{N} = (0,0,\nu), \boldsymbol{D} = (1,D,0)$ and $\boldsymbol{f}(\boldsymbol{u};\boldsymbol{\alpha}) = (\delta a m(s+\eta)/(s+1) - m, m - \theta s, 1 + \varepsilon a - \beta a m(s+\eta)/(s+1))$.

We repeated our analysis shown in the main text for the sediment accumulation model describing the formation of intertidal mussel beds, shown in (6). Like in the Klausmeier model, PTW of (6) lose their stability for decreasing bifurcation parameter (here the mussel growth rate δ) at an Eckhaus stability boundary (Fig. C.1A–B). We found that all results obtained for the Klausmeier model carry over to the mussel model. In short, we found that

- there is a delayed loss of stability phenomenon and observed time delays between PTW destabilisations and wavelength changes cover several orders of magnitude (Fig. C.1D),
- the delay is approximately memoryless to dynamics that occur before crossing the stability boundary (Fig. C.1C),
- the relation between the time delay t_{delay} and the distance to the stability boundary at the wavelength change $\delta_{\text{stab}} - \delta_{\text{change}}$ is $t_{\text{delay}} \sim (\delta_{\text{stab}} - \delta_{\text{change}})^{-2}$, but there are an order of magnitude differences in t_{delay} for different parameter change regimes (Fig. C.2A),
- the relation between the time delay t_{delay} and the accumulated distance from the stability boundary $\overline{\delta}(t)$ at the wavelength change is $t_{\text{delay}} \sim \overline{\delta}(t_{\text{stab}} + t_{\text{delay}})$, with no quantitative differences between different parameter change regimes (Fig. C.2B),
- the relation between the time delay t_{delay} maximum real part of the PTWs' essential spectra $\mu(\delta)$ is $t_{\text{delay}} \sim \mu(\delta_{\text{change}})^{-1}$ but there are

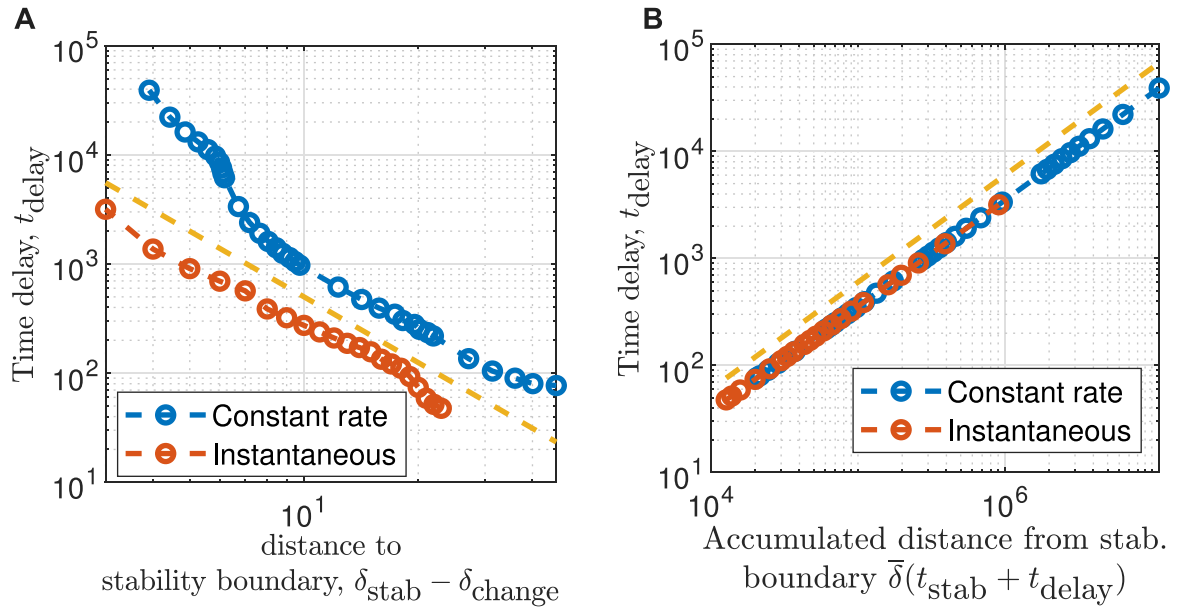

Fig. C.2. Time delay in relation to bifurcation parameter changes. **A**: The relation between the time delay t_{delay} and the distance of the bifurcation parameter δ from the stability boundary at the time of the wavelength change is shown for an instantaneous parameter change to a target value δ_{target} (red), and for a regime in which δ decreases at constant rate m (blue) (where each data point corresponds to a different value of $0.0001 \leq m \leq 0.03$). The dashed lines have slope −2. **B**: The relation between the time delay t_{delay} and the accumulated distance from the stability boundary at the time of the wavelength change, $\overline{\delta}(t_{\text{stab}} + t_{\text{delay}})$, is shown for both parameter change regimes. The dashed line has slope 1. Other parameter values are $\varepsilon = 50$, $\beta = 200$, $\eta = 0.1$, $\theta = 2.5$, $\nu = 360$, and $D = 1$.

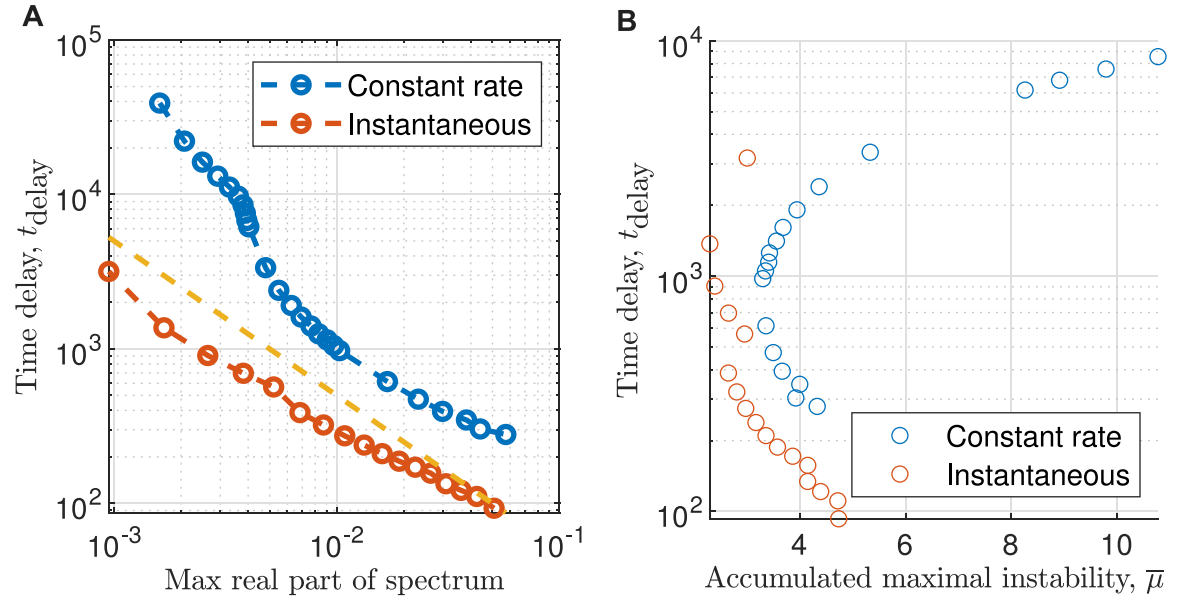

Fig. C.3. Time delay of wavelength change in relation to the maximum real part of the essential spectrum. **A**: The time delay of a wavelength change that occurs after crossing a stability boundary is compared with the maximum real part of the essential spectrum of the unstable solution at which the wavelength change occurs for instantaneous changes of the bifurcation parameter (red), and constant rates of change of the bifurcation parameter m (blue) (where each data point corresponds to a different value of $0.0001 \leq m \leq 0.03$). The dashed line has slope −1. **B**: The time delay is compared with the accumulated maximal instability for both parameter change regimes. Other parameter values are $\varepsilon = 50$, $\beta = 200$, $\eta = 0.1$, $\theta = 2.5$, $\nu = 360$, and $D = 1$.

an order of magnitude differences in t_{delay} for different parameter change regimes (Fig. C.3A),

- the accumulated maximal instability at a wavelength change $\overline{\mu}(\delta_{\text{change}}) \in I_{\overline{\mu}_{\text{change}}} \approx [3, 11]$ consistently for all parameter change regimes (Fig. C.3B).

References

Asch, A., Avery, M., Cortez, A., Scheel, A., 2024. Slow passage through the busse balloon – predicting steps on the eckhaus staircase. European J. Appl. Math. 1–26. http://dx.doi.org/10.1017/s0956792524000160.

Bastiaansen, R., Doelman, A., Eppinga, M.B., Rietkerk, M., 2020. The effect of climate change on the resilience of ecosystems with adaptive spatial pattern formation. In: Etienne, R. (Ed.), Ecol. Lett. 23 (3), 414–429. http://dx.doi.org/10.1111/ele.13449.

Bastiaansen, R., Jaïbi, O., Deblauwe, V., Eppinga, M.B., Siteur, K., Siero, E., Mermoz, S., Bouvet, A., Doelman, A., Rietkerk, M., 2018. Multistability of model and real dryland ecosystems through spatial self-organization. Proc. Natl. Acad. Sci. 11256–11261. http://dx.doi.org/10.1073/pnas.1804771115.

Bennett, J.J.R., Sherratt, J.A., 2018a. Large scale patterns in mussel beds: stripes or spots? J. Math. Biol. 78 (3), 815–835. http://dx.doi.org/10.1007/s00285-018-1293-z.

Bennett, J.J.R., Sherratt, J.A., 2018b. Long-distance seed dispersal affects the resilience of banded vegetation patterns in semi-deserts. J. Theoret. Biol. 481, 151–161. http://dx.doi.org/10.1016/j.jtbi.2018.10.002.

Bordyugov, G., Fischer, N., Engel, H., Manz, N., Steinbock, O., 2010. Anomalous dispersion in the Belousov–Zhabotinsky reaction: Experiments and modeling. Physica D 239 (11), 766–775. http://dx.doi.org/10.1016/j.physd.2009.10.022.

Britton, N.F., 1990. Spatial structures and periodic travelling waves in an integro-differential reaction-diffusion population model. SIAM J. Appl. Math. 50 (6), 1663–1688. http://dx.doi.org/10.1137/0150099.

Busse, F.H., 1978. Non-linear properties of thermal convection. Rep. Progr. Phys. 41 (12), 1929–1967. http://dx.doi.org/10.1088/0034-4885/41/12/003.

Consolo, G., Currò, C., Valenti, G., 2019. Supercritical and subcritical turing pattern formation in a hyperbolic vegetation model for flat arid environments. Phys. D 398, 141–163. http://dx.doi.org/10.1016/j.physd.2019.03.006.

Consolo, G., Valenti, G., 2019. Secondary seed dispersal in the klausmeier model of vegetation for sloped semi-arid environments. Ecol. Model. 402, 66–75. http://dx.doi.org/10.1016/j.ecolmodel.2019.02.009.

Dagbovie, A.S., Sherratt, J.A., 2014. Pattern selection and hysteresis in the rietkerk model for banded vegetation in semi-arid environments. J. R. Soc. Interface 11 (99), 20140465. http://dx.doi.org/10.1098/rsif.2014.0465.

Dakos, V., Kéfi, S., Rietkerk, M., van Nes, E.H., Scheffer, M., 2011. Slowing down in spatially patterned ecosystems at the brink of collapse. Amer. Nat. 177 (6), E153–E166. http://dx.doi.org/10.1086/659945.

Dalwadi, M.P., Pearce, P., 2023. Universal dynamics of biological pattern formation in spatio-temporal morphogen variations. Proc. R. Soc. A 479 (2271), http://dx.doi.org/10.1098/rspa.2022.0829.

De Maesschalck, P., 2008. Smoothness of transition maps in singular perturbation problems with one fast variable. J. Differential Equations 244 (6), 1448–1466.

De Maesschalck, P., Schecter, S., 2016. The entry–exit function and geometric singular perturbation theory. J. Differential Equations 260 (8), 6697–6715.

Degond, P., Diez, A., Walczak, A., 2022. Topological states and continuum model for swarmalators without force reciprocity. Anal. Appl. (Singap.) 20 (06), 1215–1270. http://dx.doi.org/10.1142/s0219530522400073.

Doedel, E.J., Oldeman, B.E., Champneys, A.R., Dercole, F., Fairgrieve, T., Kuznetsov, Y., Paenroth, R., Sandstede, B., Wang, X., Zhang, C., 2012. AUTO-07p: Continuation and Bifurcation Software for Ordinary Differential Equations. Tech. rep..

Dzianach, P.A., Dykes, G.A., Strachan, N.J.C., Forbes, K.J., Pérez-Reche, F.J., 2019. Challenges of biofilm control and utilization: lessons from mathematical modelling. J. R. Soc. Interface 16 (155), 20190042. http://dx.doi.org/10.1098/rsif.2019.0042.

Eigentler, L., 2020. Intraspecific competition in models for vegetation patterns: decrease in resilience to aridity and facilitation of species coexistence. Ecol. Complexity 42, 100835. http://dx.doi.org/10.1016/j.ecocom.2020.100835.

Eigentler, L., Sensi, M., 2024. Code repository for Eigentler and Sensi (2024) Delayed loss of stability. Zenodo, http://dx.doi.org/10.5281/ZENODO.12548663.

Eigentler, L., Sherratt, J.A., 2019. Metastability as a coexistence mechanism in a model for dryland vegetation patterns. Bull. Math. Biol. 81 (7), 2290–2322. http://dx.doi.org/10.1007/s11538-019-00606-z.

Eigentler, L., Sherratt, J.A., 2020. Spatial self-organisation enables species coexistence in a model for savanna ecosystems. J. Theoret. Biol. 487, 110122. http://dx.doi.org/10.1016/j.jtbi.2019.110122.

Eigentler, L., Sherratt, J.A., 2023. Long-range seed dispersal enables almost stationary patterns in a model for dryland vegetation. J. Math. Biol. 86 (15), http://dx.doi.org/10.1007/s00285-022-01852-x.

Gandhi, P., Iams, S., Bonetti, S., Silber, M., 2019. Vegetation pattern formation in drylands. In: Dryland Ecohydrology. Springer International Publishing, pp. 469–509.

Gourley, S.A., Chaplain, M.A.J., Davidson, F.A., 2001. Spatio-temporal pattern formation in a nonlocal reaction-diffusion equation. Dyn. Syst. 16 (2), 173–192. http://dx.doi.org/10.1080/14689360116914.

Hastings, A., Abbott, K.C., Cuddington, K., Francis, T., Gellner, G., Lai, Y.C., Morozov, A., Petrovskii, S., Scranton, K., Zeeman, M.L., 2018. Transient phenomena in ecology. Science 361 (6406), http://dx.doi.org/10.1126/science.aat6412, URL https://www.ncbi.nlm.nih.gov/pubmed/30190378.

Kaklamanos, P., Kuehn, C., Popović, N., Sensi, M., 2023. Entry–exit functions in fast–slow systems with intersecting eigenvalues. J. Dynam. Differential Equations 1–18.

Kéfi, S., Guttal, V., Brock, W.A., Carpenter, S.R., Ellison, A.M., Livina, V.N., Seekell, D.A., Scheffer, M., van Nes, E.H., Dakos, V., 2014. Early warning signals of ecological transitions: Methods for spatial patterns. In: Solé, R.V. (Ed.), PLoS ONE 9 (3), e92097. http://dx.doi.org/10.1371/journal.pone.0092097.

Klausmeier, C.A., 1999. Regular and irregular patterns in semiarid vegetation. Science 284 (5421), 1826–1828. http://dx.doi.org/10.1126/science.284.5421.1826, URL https://www.science.org/doi/10.1126/science.284.5421.1826.

Kopell, N., Howard, L.N., 1973. Plane wave solutions to reaction-diffusion equations. Stud. Appl. Math. 52 (4), 291–328. http://dx.doi.org/10.1002/sapm1973524291.

Kot, M., 1992. Discrete-time travelling waves: Ecological examples. J. Math. Biol. 30 (4), http://dx.doi.org/10.1007/bf00173295.

Liu, W., 2000. Exchange lemmas for singular perturbation problems with certain turning points. J. Differential Equations 167 (1), 134–180.

Liu, Q.-X., Herman, P.M.J., Mooij, W.M., Huisman, J., Scheffer, M., Olff, H., van de Koppel, J., 2014. Pattern formation at multiple spatial scales drives the resilience of mussel bed ecosystems. Nature Commun. 5 (1), http://dx.doi.org/10.1038/ncomms6234.

Liu, Q.-X., Weerman, E.J., Herman, P.M.J., Olff, H., van de Koppel, J., 2012. Alternative mechanisms alter the emergent properties of self-organization in mussel beds. Proc. R. Soc. Lond. B. 279 (1739), 2744–2753. http://dx.doi.org/10.1098/rspb.2012.0157.

Marasco, A., Iuorio, A., Carteni, F., Bonanomi, G., Tartakovsky, D.M., Mazzoleni, S., Giannino, F., 2014. Vegetation pattern formation due to interactions between water availability and toxicity in plant–soil feedback. Bull. Math. Biol. 76 (11), 2866–2883. http://dx.doi.org/10.1007/s11538-014-0036-6.

Meron, E., 2016. Pattern formation - a missing link in the study of ecosystem response to environmental changes. Math. Biosci. 271, 1–18. http://dx.doi.org/10.1016/j.mbs.2015.10.015.

Meron, E., Gilad, E., von Hardenberg, J., Shachak, M., Zarmi, Y., 2004. Vegetation patterns along a rainfall gradient. Chaos Solitons Fractals 19 (2), 367–376. http://dx.doi.org/10.1016/s0960-0779(03)00049-3.

Neishtadt, A.I., 1987. Persistence of stability loss for dynamical bifurcations I. Differ. Equ. 23, 1385–1391.

Pinto-Ramos, D., Clerc, M.G., Tlidi, M., 2023. Topological defects law for migrating banded vegetation patterns in arid climates. Sci. Adv. 9 (31), http://dx.doi.org/10.1126/sciadv.adf6620.

Pontin, D.I., Priest, E.R., 2022. Magnetic reconnection: MHD theory and modelling. Living Rev. Sol. Phys. 19 (1), http://dx.doi.org/10.1007/s41116-022-00032-9.

Proctor, M., Tobias, S., Knobloch, E., 2000. Noise-sustained structures due to convective instability in finite domains. Physica D 145 (3–4), 191–206. http://dx.doi.org/10.1016/s0167-2789(00)00127-5.

Rademacher, J.D., Sandstede, B., Scheel, A., 2007. Computing absolute and essential spectra using continuation. Phys. D 229 (2), 166–183. http://dx.doi.org/10.1016/j.physd.2007.03.016.

Rietkerk, M., Bastiaansen, R., Banerjee, S., van de Koppel, J., Baudena, M., Doelman, A., 2021. Evasion of tipping in complex systems through spatial pattern formation. Science 374 (6564), http://dx.doi.org/10.1126/science.abj0359.

Rietkerk, M., van de Koppel, J., 2008. Regular pattern formation in real ecosystems. Trends Ecol. Evol. 23 (3), 169–175. http://dx.doi.org/10.1016/j.tree.2007.10.013.

Scheffer, M., Bascompte, J., Brock, W.A., Brovkin, V., Carpenter, S.R., Dakos, V., Held, H., van Nes, E.H., Rietkerk, M., Sugihara, G., 2009. Early-warning signals for critical transitions. Nature 461 (7260), 53–59. http://dx.doi.org/10.1038/nature08227.

Shen, Z., Wei, J., 2020. Stationary pattern of a reaction–diffusion Mussel–Algae model. Bull. Math. Biol. 82 (4), http://dx.doi.org/10.1007/s11538-020-00727-w.

Sherratt, J.A., 1996. Periodic travelling waves in a family of deterministic cellular automata. Physica D 95 (3–4), 319–335. http://dx.doi.org/10.1016/0167-2789(96)00070-x.

Sherratt, J.A., 2005. An analysis of vegetation stripe formation in semi-arid landscapes. J. Math. Biol. 51 (2), 183–197. http://dx.doi.org/10.1007/s00285-005-0319-5.

Sherratt, J.A., 2010. Pattern solutions of the klausmeier model for banded vegetation in semi-arid environments I. Nonlinearity 23 (10), 2657–2675. http://dx.doi.org/10.1088/0951-7715/23/10/016.

Sherratt, J.A., 2011. Pattern solutions of the klausmeier model for banded vegetation in semi-arid environments II: patterns with the largest possible propagation speeds. Proc. R. Soc. Lond. Ser. A Math. Phys. Eng. Sci. 467 (2135), 3272–3294. http://dx.doi.org/10.1098/rspa.2011.0194.

Sherratt, J.A., 2012. Numerical continuation methods for studying periodic travelling wave (wavetrain) solutions of partial differential equations. Appl. Math. Comput. 218 (9), 4684–4694. http://dx.doi.org/10.1016/j.amc.2011.11.005.

Sherratt, J.A., 2013a. History-dependent patterns of whole ecosystems. Ecol. Complexity 14, 8–20. http://dx.doi.org/10.1016/j.ecocom.2012.12.002.

Sherratt, J.A., 2013b. Numerical continuation of boundaries in parameter space between stable and unstable periodic travelling wave (wavetrain) solutions of partial differential equations. Adv. Comput. Math. 39 (1), 175–192. http://dx.doi.org/10.1007/s10444-012-9273-0.

Sherratt, J.A., 2013c. Pattern solutions of the klausmeier model for banded vegetation in semi-arid environments III: The transition between homoclinic solutions. Phys. D 242 (1), 30–41. http://dx.doi.org/10.1016/j.physd.2012.08.014.

Sherratt, J.A., 2013d. Pattern solutions of the klausmeier model for banded vegetation in semiarid environments IV: Slowly moving patterns and their stability. SIAM J. Appl. Math. 73 (1), 330–350. http://dx.doi.org/10.1137/120862648.

Sherratt, J.A., 2013e. Pattern solutions of the klausmeier model for banded vegetation in semiarid environments v: The transition from patterns to desert. SIAM J. Appl. Math. 73 (4), 1347–1367. http://dx.doi.org/10.1137/120899510.

Sherratt, J., 2016. Using numerical bifurcation analysis to study pattern formation in mussel beds. In: Morozov, A., Ptashnyk, M., Volpert, V. (Eds.), Math. Model. Nat. Phenom. 11 (5), 86–102. http://dx.doi.org/10.1051/mmnp/201611506.

Sherratt, J.A., Liu, Q.-X., van de Koppel, J., 2021. A comparison of the "reduced losses" and "increased production" models for mussel bed dynamics. Bull. Math. Biol. 83 (10), http://dx.doi.org/10.1007/s11538-021-00932-1.

Sherratt, J.A., Lord, G.J., 2007. Nonlinear dynamics and pattern bifurcations in a model for vegetation stripes in semi-arid environments. Theor. Popul. Biol. 71 (1), 1–11. http://dx.doi.org/10.1016/j.tpb.2006.07.009.

Sherratt, J.A., Mackenzie, J.J., 2016. How does tidal flow affect pattern formation in mussel beds? J. Theoret. Biol. 406, 83–92. http://dx.doi.org/10.1016/j.jtbi.2016.06.025.

Siero, E., 2018. Nonlocal grazing in patterned ecosystems. J. Theoret. Biol. 436, 64–71. http://dx.doi.org/10.1016/j.jtbi.2017.10.001.

Siero, E., Siteur, K., Doelman, A., van de Koppel, J., Rietkerk, M., Eppinga, M.B., 2019. Grazing away the resilience of patterned ecosystems. Amer. Nat. 193 (3), 472–480. http://dx.doi.org/10.1086/701669.

Siteur, K., Siero, E., Eppinga, M.B., Rademacher, J.D., Doelman, A., Rietkerk, M., 2014. Beyond turing: The response of patterned ecosystems to environmental change. Ecol. Complexity 20, 81–96. http://dx.doi.org/10.1016/j.ecocom.2014.09.002.

United Nations Convention to Combat Desertification, 2017. The Global Land Outlook. Bonn, Germany.

van de Koppel, J., Rietkerk, M., Dankers, N., Herman, P.M.J., 2005. Scale-dependent feedback and regular spatial patterns in Young mussel beds. Amer. Nat. 165 (3), E66–E77. http://dx.doi.org/10.1086/428362.

van der Stelt, S., Doelman, A., Hek, G., Rademacher, J.D.M., 2013. Rise and fall of periodic patterns for a generalized Klausmeier–Gray–Scott model. J. Nonlinear. Sci. 23 (1), 39–95. http://dx.doi.org/10.1007/s00332-012-9139-0.

van Hecke, M., 2003. Coherent and incoherent structures in systems described by the 1d CGLE: experiments and identification. Physica D 174 (1–4), 134–151. http://dx.doi.org/10.1016/s0167-2789(02)00687-5.

von Hardenberg, J., Meron, E., Shachak, M., Zarmi, Y., 2001. Diversity of vegetation patterns and desertification. Phys. Rev. Lett. 87, 198101. http://dx.doi.org/10.1103/PhysRevLett.87.198101.

Wang, X., Zhang, G., 2018. Vegetation pattern formation in seminal systems due to internal competition reaction between plants. J. Theoret. Biol. 458, 10–14. http://dx.doi.org/10.1016/j.jtbi.2018.08.043.

Wang, X., Zhang, G., 2019. The influence of infiltration feedback on the characteristic of banded vegetation pattern on hillsides of semiarid area. PLOS ONE 14 (1), e0205715. http://dx.doi.org/10.1371/journal.pone.0205715.

Zelnik, Y.R., Kinast, S., Yizhaq, H., Bel, G., Meron, E., 2013. Regime shifts in models of dryland vegetation. Philos. Trans. R. Soc. London, Ser. A 371 (2004), 20120358. http://dx.doi.org/10.1098/rsta.2012.0358.